STRUCTURAL FEATURES AND THE REACTION MECHANISM OF CYTOCHROME OXIDASE

IRON AND COPPER X-RAY ABSORPTION FINE STRUCTURE

L. POWERS, B. CHANCE, Y. CHING, AND P. ANGIOLILLO, *Bell Telephone Laboratories, Murray Hill, New Jersey 07974, and Johnson Research Foundation, University of Pennsylvania, Philadelphia, Pennsylvania 19104*

ABSTRACT X-ray edge absorption of copper and extended fine structure studies of both copper and iron centers have been made of cytochrome oxidase from beef heart, *Paracoccus dentrificans*, and HB-8 thermophilic bacteria (1–2.5 mM in heme). The desired redox state (fully oxidized, reduced CO, mixed valence formate and CO) in the x-ray beam was controlled by low temperature (−140°C) and was continuously monitored by simultaneous optical spectroscopy and by electron paramagnetic resonance (EPR) monitoring every 30 min of x-ray exposure. The structure of the active site, a cytochrome a_3-copper pair in fully oxidized and in mixed valence formate states where they are spin coupled, contains a sulphur bridge with three ligands 2.60 ± 0.03 Å from Fe_{a_3} and 2.18 ± 0.03 Å from Cu_{a_3}. The distance between Fe_{a_3} and Cu_{a_3} is 3.75 ± 0.05 Å, making the sulphur bond angle 103° reasonable for sp^3 sulphur bonding. The Fe_{a_3} first shell has four typical heme nitrogens (2.01 ± 0.03 Å) with a proximal nitrogen at 2.14 ± 0.03 Å. The sixth ligand is the bridging sulphur. The Cu_{a_3} first shell is identical to oxidized stellacyanin containing two nitrogens and a bridging sulphur. Upon reduction with CO, the active site is identical to reduced stellacyanin for the Cu_{a_3} first shell and contains the sulphur that forms the bridge in fully oxidized and mixed valence formate states. The Fe_{a_3} first shell is identical to oxyhemoglobin but has CO instead of O_2. The other redox centers, Fe_a and the other "EPR detectable" Cu are not observed in higher shells of Fe_{a_3}. Fe_a has six equidistant nitrogens and Cu_a has one (or two) nitrogens and three (or two) sulphurs with typical distances; these ligands change only slight on reduction. These structures afford the basis for an oxygen reduction mechanism involving oxy- and peroxy intermediates.

INTRODUCTION

The remarkable effectiveness of the binuclear iron-copper complex of the active site of cytochrome oxidase in reducing oxygen to water with a minimum release of free radical intermediates on the one hand, and a maximum efficiency of energy conservation on the other, has remained one of the mysteries of modern biology. Significant steps forward in our knowledge of cytochrome oxidase were made by Warburg in 1929 (1), who identified the remarkable "green heme"; by Keilin (2), who identified Warburg's green heme and MacMunn's histohemins as cytochromes; by Wharton and Tzagoloff (3), who found copper to be an essential component of the oxidase; and by those who found the metal centers functional in ozygen reduction in isolated mitochondria (4) and in the purified enzyme (5). However, detailed studies of the oxidase were continually rendered difficult by the presence of duplicate iron and copper atoms[1] and the absorption band overlap. In addition, the magnetic properties

[1] a_3 heme and Cu_{a_3} are identified with the active site of the oxidase, whereas Fe_{a_3} refers specifically to the iron atom of a_3 heme. Correspondingly, a heme and Cu_a refer to the electron reservoir component of the oxidase.

were rendered intractable to conventional microwave electron paramagnetic resonance (EPR) by their spin coupling (6). Kinetic resolution of the two pairs of components by flow flash (5), room temperature rapid flow (4), and by freeze techniques (7) revealed many facets of the functions of the metal atoms in oxidation-reduction reactions and determined the sequence with which the components react, both with cytochrome *c* in reduction and oxygen in oxidation (8). However, the time separation of the reactions is small, and no discernible oxygen-reduction intermediates were identified.

Caging of the iron atom by CO against the oxygen reaction, then rapidly initiating ligand exchange by flash photolysis, is a technique that was outlined by Hartridge and Roughton (9) in their remarkable study of oxy- and carboxy hemoglobin. Shortly after the discovery of the photolysis of cytochrome oxidase CO (10), Gibson et al. (5) used flash-flow photolysis of the CO compound in the presence of rapidly mixed oxygen to obtain kinetic data on cytochrome oxidase. In the course of these studies, they demonstrated clearly that the reaction of recently photolyzed oxidase with oxygen is identical in its kinetic parameters to that of the fully reduced CO-free species. Flash photolysis of CO compounds of cytochrome oxidase, myoglobin, and hemoglobin has been studied by Chance et al. (11). The caged oxidase has been flash photolyzed in the presence of oxygen at low temperatures using a technique termed "triple trapping" (12). The key to this method has been the mixing of oxygen with cytochrome oxidase-CO in aprotic solvents at $-25°C$, a temperature so low that dissociation of CO from the oxidase in the dark occurs at a negligible rate; thus no oxygen reaction can occur after freeze trapping of the oxygenated mixture.

Subsequently, flash photolysis and ligand exchange can occur over a wide range of temperatures, and the activation energies of intermediate steps are larger than that in the oxygen reaction. Three intermediates have been identified: an oxycompound (*A*) and two kinds of oxygen-reduction compounds (*B* and *C*) (13–15), involving partly and fully oxidized Fe_{a_3} and Cu_{a_3}. The latter causes the oxidation of the electron transmitter components, Fe_a and Cu_a. These studies identified all four metal atoms as having appropriate functions in the oxidation-reduction reaction and focused attention upon the binuclear complex a_3 heme-Cu_{a_3} as the functional prosthetic group of the enzyme, overthrowing both the "unitary theory" of cytochrome oxidase function (16), and the concerted action hypothesis for cytochrome oxidase function (17). This rendered much of the action of cytochrome oxidase interpretable on the basis of what was already known about the reaction of iron porphyrin proteins with oxygen (18), the reaction of the binuclear copper-copper complex hemocyanin with oxygen (19), and the reaction of catalase with peroxides (20).

A consequence of the low temperature experiments was the discovery that the active site of cytochrome oxidase consisted of the closely coupled binuclear complex, Fe_{a_3}-Cu_{a_3}. The structure of this complex must hold the key for rapid and effective combination with oxygen and consequent reduction of oxygen to water by electron transfer from copper and iron. The particular geometry that makes this possible has been the point of speculation by a number of authors, including Blumberg and Peisach (21) and Powers et al. (22), who considered that the μ-oxo (oxygen atom bridged structure) would be appropriate to a closely coupled iron-copper binuclear complex. To this point, Babcock et al. in their recent paper (23) suggested that this might be ligand *B* which links the iron and copper. These proposals superceded the histidine bridge put forward by Palmer et al. (24).

A suggestion for the possible distance of iron and copper in the binuclear complex was afforded by the work of Brown et al. (19) on hemocyanin, where they found the distance between the two copper atoms in the oxy form to be 3.68 ± 0.05 Å. The key point provided by this model is that oxygen once bound in the cuprous-cuprous complex is reduced to the level of peroxide by electron transfer from copper, yielding a cupric-cupric bridged peroxide complex (19). The parallel between oxyhemocyanin and compound *B* of cytochrome oxidase, in which one iron replaces one copper in the binuclear peroxide intermediate, is compelling.

These kinetic and mechanistic studies have intensified interest in the nature of the active form of cytochrome oxidase, the state of the metal atoms, and if possible, conformation changes that might occur in the redox cycle. The inability of magnetic methods to deal with the copper component, or indeed, to give interpretable data on the iron component, led to the studies of cytochrome oxidase with the recently accessible tunable high intensity x-ray sources available from synchrotrons (25). Two types of approaches are relevant to cytochrome oxidase.

The first is K-edge absorption, where 1s electron transitions to unoccupied bound states shift characteristically with redox changes and are related to the associated change in charge density of the metal atom. Recent studies (22) identified edge contributions of each copper site in the oxidized and reduced states using appropriate models from investigation of the oxidized, reduced, and the two mixed valence hybrids (mixed valence CO and mixed valence formate). The electron reservoir portion, Cu_a, was shown to have a more covalent environment than the copper redox component of the active site, Cu_{a_3}. The latter is nicely fitted to stellacyanin (22), whereas N(O) and S^- were suggested as possible ligands for Cu_a. The stellacyanin analogy was later supported by the homology between the amino acid sequence of subunit II and that of the type I "blue" copper proteins (26).

The second type of approach is that of extended x-ray absorption fine structure (EXAFS). These are fluctuations in the x-ray absorption spectrum that occur when the energy of the incident radiation exceeds the ionization potential and result from the interference of the emitted photoelectrons and those backscattered from neighboring atoms of the iron or copper absorber. This interference function allows calculation of the average distances from the absorber to the nearby neighboring atoms. The signal-to-noise ratio of the measurements is directly proportional to the concentration of absorbing atoms, and satisfactory measurements have been obtained for highly concentrated (7–20 mM) biological preparations (19, 27). These concentrations are not possible for cytochrome oxidase, however, and special preparation techniques were developed to obtain 1–1.5-mM concentrations. In addition, two x-ray fluorescence detection systems were fabricated to obtain maximum signal-to-noise ratio in this study.

Prominent among the experimental difficulties is the preparation of fully occupied samples of cytochrome oxidase at maximal concentrations (~1.5 mM). First, details on these preparation methods are not available elsewhere and thus form a considerable part of this presentation for appropriate authentication of the sample. Second, room temperature irradiation of cytochrome oxidase by the intense x-ray beam caused its rapid reduction by hydrated electrons, at the rate of ~2 μM/s (28). Therefore, the development of an appropriate cryostat, online optical monitoring spectrophotometer, and an offline EPR monitoring apparatus, to monitor samples immediately before, during, and after irradiation in the same sample holder

at temperatures low enough to immobilize hydrated electrons, permitted us to study fully occupied, well characterized, and quantitated redox states.

EXAFS experiments are often characterized by inadequate control of the state of the enzyme during irradiation; this has made the identification of the results with known redox states impossible. Consequently, this paper reports sample preparation, technical methods, and experimental results of Fe and Cu in highly concentrated solubilized cytochrome oxidase from beef heart and other sources, together with the structure and corresponding mechanism for the oxygen reduction by the enzyme. Preliminary reports are published elsewhere (29).

METHODS

Biochemical Preparation

The preparation differed from those in our previous studies (22) and appropriate details are therefore given below. Cytochrome *c* oxidase (1 g of protein) was prepared according to Yonetani's method (30). Two to four ammonium sulfate fractions between 26 and 34% were used to achieve optimum purity as displayed by the oxidized and dithionite reduced spectra of Fig. 1; the purity criteria were determined from absorbance ratios: (*a*) 445 nm (reduced)/424 nm (reduced) = 2.4 (30), (*b*) 445 nm (reduced)/422 nm (oxidized) = 1.30–1.40 (30), (*c*) 280 nm (oxidized)/445 nm (reduced) = 2.0–2.4 (30), (*d*) purified oxidase contains 8–10 nmole of a heme/mg of protein, (*e*) adventitious Cu (~5%) as determined by the ratio of total copper (atomic absorption assay) to heme as determined spectroscopically.

The concentration of oxidase in the samples prepared for the EXAFS studies could not be determined precisely by optical or electron paramagnetic resonance (EPR) observations. Therefore, a sample packed in a precisely determined volume (9.51 μl) was dissolved in 7 ml of 2% cholate and 50 mM phosphate buffer (pH 7.4). The absorbance was determined at 600 nm and the concentration was calculated to be 1.10 mM, $\epsilon = 24\ mM^{-1} \times cm^{-1}$, characteristic of an average sample. This was exceeded by ~20% in the most concentrated ones and fell by ~30% for some of the derivatives to which chemicals were added as in the mixed valence states.

EXAFS Samples of Cytochrome Oxidase

The purified oxidase at ~300 μM concentration in 2% cholate and 50 mM phosphate buffer was dialyzed against 0.25% cholate in 15 mM phosphate buffer for 12 h. The preparation was concentrated to ~1.0 mM under vacuum and stored in liquid nitrogen.

RESTING OXIDASE The purified oxidase was further concentrated by evaporating more water from successive layers under a stream of air (usually to ~1.3 mM hydrated oxidase), tightly packed in an EXAFS sample holder, and stored in liquid nitrogen.

FULLY REDUCED CO OXIDASE The procedure is carried out in a CO-filled glove bag at room

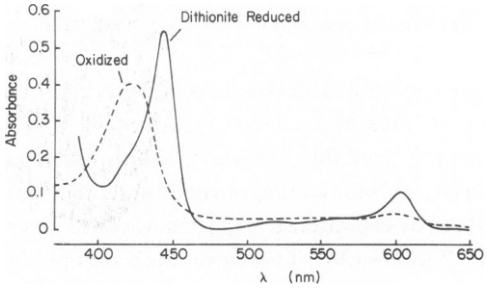

FIGURE 1 Optical transmission spectra of oxidized and sodium dithionite-reduced cytochrome *c* oxidase (~300 μM).

temperature. Diaminodurene (DAD) and phenazine methosulfate (PMS) were used as mediators and added at a final concentration of 100 μM each. The sample was then incubated for 30 min. NADH was added to a final concentration of 10 mM, and a further incubation for 60 min occurred. A second aliquot of NADH (10 mM) was added, and the sample was incubated for another 60 min. The low temperature reflectance spectrum of the sample was then monitored and further NADH additions and 30-min incubations were repeated until both the 830 and the 655 nm peaks, corresponding, respectively, to the oxidized copper and the oxidized a_3 heme components, had disappeared. If incomplete reduction was observed after repeating this procedure several times, a very small amount of solid sodium dithionite was added and the preparation was incubated for 30 min. This latter treatment ensured complete reduction of mixed valence states that were present (see below: CO MIXED VALENCE SAMPLES).

FORMATE MIXED VALENCE SAMPLES These operations were carried out in air at room temperature. 1 M formate solution was added to the concentrated oxidase to achieve final concentration of 30 mM. The preparation was incubated at room temperature under nitrogen for 30 min. DAD and PMS were then added to a final concentration of 50 μM each. NADH was added to the sample to a 7-mM final concentration and incubated for 30 min at room temperature under nitrogen. Another equal addition of NADH was added, and the sample was incubated for another 30 min. The low temperature reflectance spectrum was then monitored and the 830-nm transition had disappeared completely without affecting the 655-nm transition. The sample was immediately stored in liquid nitrogen.

CO MIXED VALENCE SAMPLES The procedure of case 2 was carried through to the fully reduced state, and the sample was left in the CO-filled glove bag 8–12 h. Under these conditions, there was a slow approach to a redox equilibrium of the system that involved a slow reoxidation of the *a* heme and Cu_a. Spectroscopic monitoring of the 830-nm copper absorption band and the 605-nm heme absorption band showed that Cu_a and *a* heme became fully oxidized in this interval. EPR was also used to ascertain oxidation of *a* heme ($g = 3.05$) and copper ($g = 2.0$). Some water was evaporated during the process, and the final concentration of the oxidase was ~1.5 mM. The sample was then frozen in liquid nitrogen under a CO atmosphere.

Cytochrome Oxidases from Sources other than Beef Heart

Cytochrome oxidase containing two small subunits has been prepared both from *Paracoccus denitrificans* bacteria (31) and from the thermophilic bacterium HB-8 (32). These preparations were suitable for iron and copper EXAFS and for copper EXAFS, respectively. In the latter case, the presence of

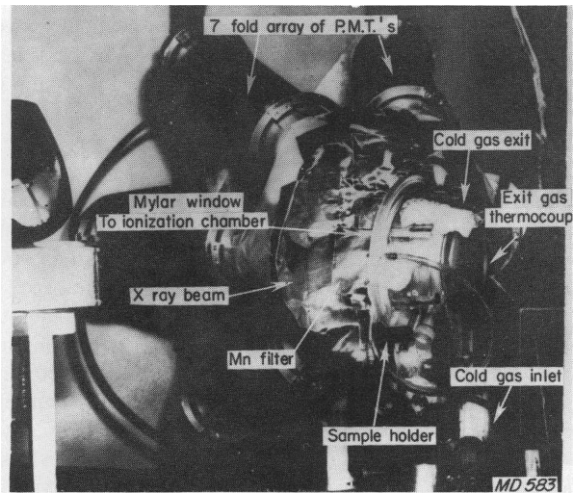

FIGURE 2 Scintillation detector array and low temperature cryostat as arranged at SSRL Beam line EXAFS I.

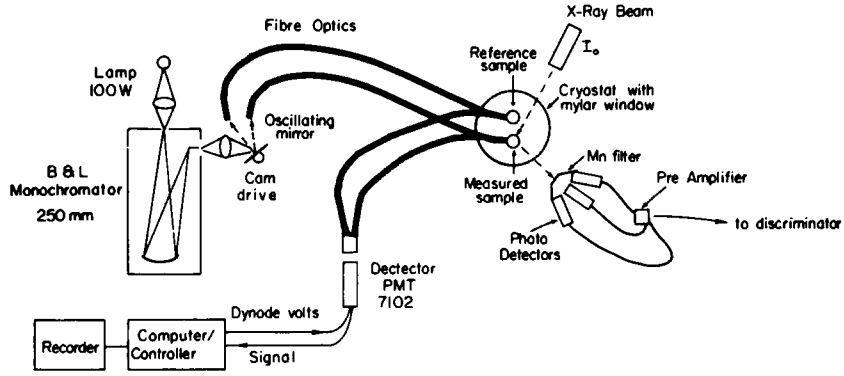

FIGURE 3 Reflectance split-beam spectrophotometer as arranged at SSRL for online monitoring PMT, photomultiplier tube.

cytochrome *c* precluded studies of iron EXAFS. The concentrations of these preparations equalled those obtainable from beef heart and were assayed by optical and EPR observations. Reductions were carried out as described above.

Monitoring

The methods are divided into two sections: biophysical and biochemical devices. Most important among the biophysical devices has been the development of an efficient method for low temperature observation of the edge and EXAFS signals.

LOW TEMPERATURE CRYOSTAT To maintain the sample at a uniform low temperature using liquid nitrogen (and not helium), a cryostat has been developed that maintains the samples in a flow of temperature-regulated nitrogen (down to −140°C) and at the same time permits hemispherical exposure of the sample for excitation by the x-ray beam and collection of the sample fluorescence. Furthermore, the cryostat has an insert for reflectance spectroscopy on the backside allowing online optical monitoring. The cryostat can be used as well for x-ray absorption studies by transmission when desirable, since the back plate is removable. This cryostat located inside the hutch is shown in Figs. 2 and 3.

LOW TEMPERATURE SAMPLE HOLDER Two types of sample holders are used, depending upon whether Stanford Synchrotron Radiation Laboratory beam line II-3 or I-5 is used. The former utilizes an oval sample area 5 × 11 × 2 mm deep, while the later is 28 × 2 × 3 mm deep. These shapes are appropriate for impingement of the whole x-ray beam upon sample material. The depth of 2 mm is appropriate for iron and copper fluorescence measurements. Lucite was found to be free of iron and copper, unlike all available aluminum.

The sample holders were made 7 mm wide and 7 cm long so that they could be inserted into the chamber of the cryostat for online reflectance spectrophotometry, into the sample holder of an offline low temperature spectrophotometer, and into the 8-mm-wide bore Scanlon dewar (James F. Scanlon Co., Solvang, Calif.) for the Varian EPR spectrometer (Varian Associates, Inc., Palo Alto, Calif.).

ONLINE MONITORING SPECTROPHOTOMETER Light-guide coupling to the backside of the sample during irradiation by the x-ray beam affords online sample monitoring in the typical split beam or "double beam" mode, where a single wavelength irradiates sample and reference material alternately (22, 33). The cryostat accommodates two identical cytochrome oxidase samples, one irradiated, the other unexposed. This allows a precise measurement by difference spectroscopy of any changes due to irradiation. If desired, an absolute standard, usually a nonreflecting spectroscopically flat material (black tape), may be used as an initial calibration for obtaining absolute spectra. Illumination of the fibers is obtained from a tungsten lamp, through a 250-mm focus B & L grating monochromator with 600 lines/mm and an infrared blazed grating (Fig. 3). The single wavelength output is shared between

the two samples at 30Hz (22, 23). A computer-controlled demodulation system memorizes the initial difference between the two identical samples and plots subsequent changes against this initial base line with relative error ±1%; alternatively, an absolute spectrum is recorded before irradiation and may be subtracted from that obtained during or after irradiation, affording a continuous record of the sample properties. Reduction of cytochrome oxidase is indicated by increased absorbance at 605 nm or decreased absorbance at 830 nm. Changes that are 10% of the initial value invalidate the sample and require its replacement with a fresh one.

EPR OBSERVATIONS Spectra were obtained on a Varian E-4 spectrometer equipped with a Scanlon wide-bore liquid helium-flow dewar. Temperatures were determined by calibrated carbon resistors. Most spectra were recorded at temperatures ~10°K at powers in the range of 5–10 mW at a modulation amplitude of 1 mT. Samples were evaluated offline before irradiation and at appropriate intervals during irradiation, (usually every 30 min) or particularly when the optical monitor indicated a perturbation. With oxidized cytochrome oxidase, the gain $g = 3.0$ and the $g = 2.0$ regions were diagnostic for sample damage, e.g., reduction of redox centers and for the production of trapped radicals (34).

X-RAY ABSORPTION OBSERVATIONS The x-ray absorption data itself can be used to evaluate alterations in the irradiated sample, although the information in this case is realized too late to be of immediate use. The lack of online data analysis prevents effective use of this method in preserving the authenticity of the biological materials. Results reported in detail elsewhere (22, 28) indicate that the edge absorption is altered by reduction of the enzyme and that irradiation > -50°C for prolonged intervals (30–60–90 min) caused peaks in the Fourier transformed data, which are not observed in these studies of authentic samples.

FUNCTIONAL ASSAY Enzymatic tests of the function of cytochrome oxidase (34) after irradiation have been made, and the activity of the preparation irradiated for over an hour under temperatures between -100 and -140°C was observed to decrease <10% with respect to the control. Thus, the main effect of the hydrated electrons is to cause redox changes rather than irreversible changes of enzyme activity during these exposure periods. The possibility that the enzyme activity in the actual sample holder under irradiation may have been suppressed beyond the recovered on dilution and enzymatic test is not precluded, and online optical monitoring is preferable.

X-Ray Absorption Techniques

MEASUREMENTS All absorption measurements were recorded at Stanford Synchrotron Radiation Laboratories (SSRL) during dedicated operation of the SPEAR storage ring, providing 40–80 mA electron beams at 3.0 GeV (36). Beam line I-5 was used for copper edge and EXAFS measurements and provided $\sim 1 \times 10^{10}$ photons/s with ~1-eV resolution. Beam line II-3 (focused) was used for iron EXAFS measurements providing $\sim 6 \times 10^{11}$ photons/s with ~7-eV resolution. For most of the spectra, however, the mirror was raised to an appropriate position to give ~3-eV resolution, causing two-to-threefold drop of the beam intensity.

The x-ray beam position and initial intensity I_0 were monitored by an ionization chamber, after a defining slit indicated changes of vertical displacement occasioned by beam steering or low frequency modulations of the x-ray beam intensity caused by uncontrollable changes of the mode of Stanford Positron-Electron Annihilator Ring (SPEAR) operation. Thus, intervals of operation at statistical noise limitation $(\text{count rate})^{1/2}$ were often interspersed with those of three-to-four times larger fluctuations.

The fluorescence, F, emitted by the sample was collected by either a filter-scintillation counter similar to that reported by Stern and Heald (37) or the LiF crystal focusing array-solid state intrinsic germanium detector as described by Marcus et al. (38).

The scintillation counters were constructed of Pilot B plastic scintillation material (Nuclear Enterprises, Inc., San Carlos, Calif.). This material has a decay time of 1.8 ns and the detectors consisted of an EMI 9813B eleven stage end-on photomultiplier (EMI Gencom, Inc., Plainview, N.Y.) to which a 2-in Diam and 2-in thick (~three absorption lengths at 8 KeV) Pilot B plastic scintillator was attached.

Spectral response of the tube was maximal at 408 nm, appropriate to the scintillator emission. The

assembly was mounted in a light-tight tubular housing, and the photomultiplier was protected from stray light by thin aluminized mylar film. Seven such counters were mounted in an array equidistant from the sample with a detector-sample geometry shown in Fig. 2. To equalize the sensitivity of the seven tubes, the total dynode voltage applied to each was varied by a potentiometer. The equalized output signals were summed in a 50-Ω resistor, and a "leading edge" discriminator was used to remove the background. A common discriminator level was thus appropriate for the summed output. Counting of the TTL output was obtained by a 6-channel hex scaler of 50-MHz capability, and the data were recorded in a PDP11/03 computer (Digital Equipment Corporation, Boston, Mass.). The length of the cable from the output of each tube to the summing resistor was adjusted so that simultaneous signals from all seven tubes produced by a single SPEAR pulse would arrive at the discriminator at sufficiently delayed times to be counted individually. This avoided duplication of amplifiers and analyzers/discriminators customarily used, and in addition, provided efficient fluorescence detection at counting rates of 1 MHz/tube with the capability to count up to the SPEAR ring frequency (~5 MHz).

As demonstrated by Stern and Heald (37), the use of a filter material that absorbs most of the elastically scattered radiation but little of the K fluorescence improves the signal-to-noise of this method:

$$\frac{S}{N} = \frac{I_{fss}}{(I_{fss} + I_{ts} + I_{fa})^{1/2}}$$

where I_{fss} is the intensity of sample fluorescence transmitted by the filter; I_{ts} is elastically scattered radiation transmitted by the filter; and I_{fa} is fluorescence from the filter caused by the absorption of radiation from the sample. The geometric factors are such that when the filter size is just large enough to

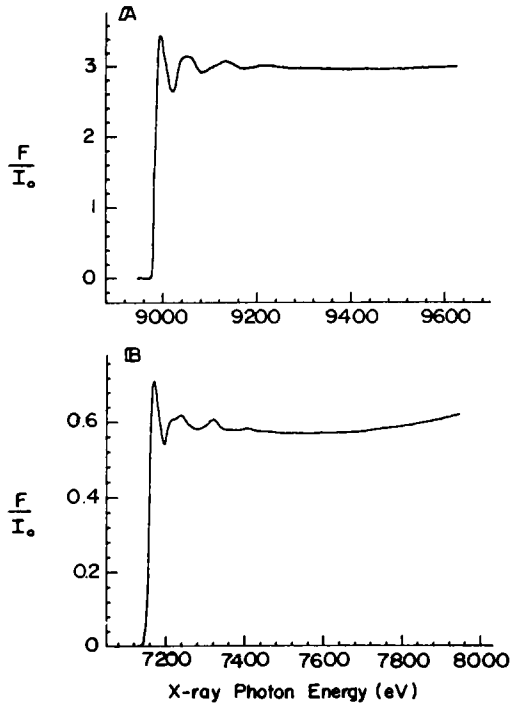

FIGURE 4 X-ray absorption spectra of cytochrome oxidase in the fully oxidized state. A linear background has been removed, which sets the absorption below the edge to zero. Data were collected by fluorescence, F, and I_0 is the incident intensity. *A*, copper; *B*, iron data.

intercept photons originating at the sample that would normally arrive at the detector, then I_{fa} is smaller when the filter is closer to the sample than to the detector. This is because the filter fluorescence is emitted in a spherical distribution and the sample size is much smaller than that of the detector array, making the solid angle of collection (I_{fa}) smaller when the filter is further from the detector array. Likewise, other terms in the denominator of the equation can be minimized to give the best S/N. The optimal values of filter properties together with size and solid-angle collection can thus be determined within experimental limitations. To reduce the counts from radiation scattered throughout the hutch, lead was used as a housing around the assembly because fluorescence from copper and iron impurities in metals such as aluminum causes additional background. This design gave a signal-to-background of 4/1 for 1 mM cytochrome oxidase at count rates of 0.4 MHz. Most of the data reported here were collected using this detection arrangement.

Energy discrimination between the K fluorescence and elastic scattering can be achieved by solid state detectors such as intrinsic germanium. These have a resolution of ~200 eV at 7 KeV but are not capable

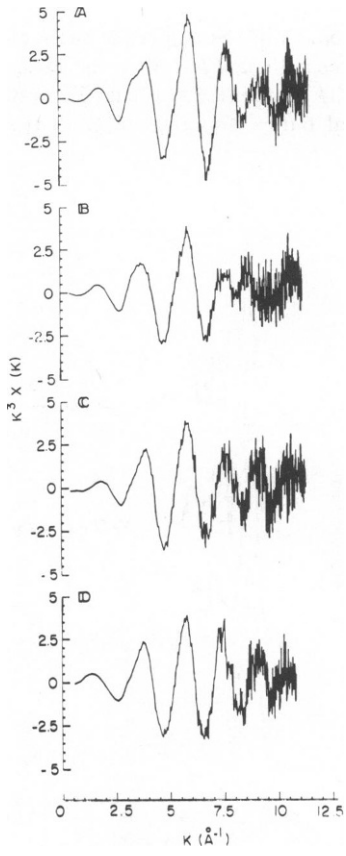

FIGURE 5

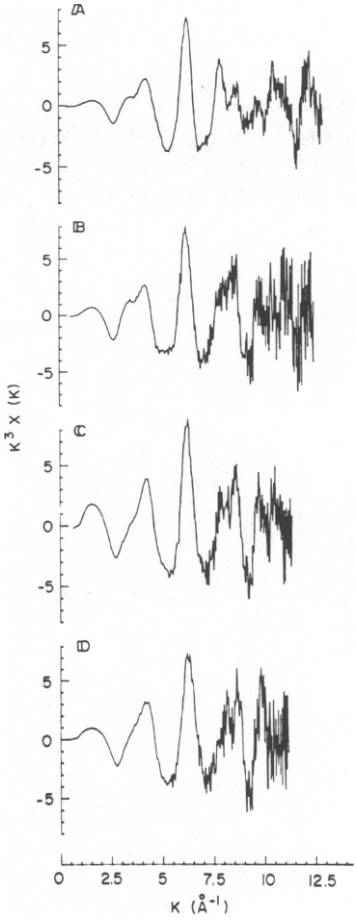

FIGURE 6

FIGURE 5 Background removed copper EXAFS data multiplied by k^3 and normalized to one copper atom of the *A*, fully oxidized; *B*, mixed valence formate; *C*, mixed valence CO; and *D*, reduced CO states.
FIGURE 6 Background removed iron EXAFS data multiplied by k^3 and normalized to one iron atom of the *A*, fully oxidized; *B*, mixed valence formate; *C*, mixed valence CO; and *D*, reduced CO states.

of high count rates (~25 kHz). To gather a large solid angle of fluorescence radiation from the sample, focusing lenses are employed, such as the above-mentioned LiF crystal array (38), which discriminate between fluorescence and elastic scattering and focus mainly the K_α fluorescence on to the intrinsic germanium detector. This array is capable of discriminating by $10^4/1$ the scattered to fluorescence photons produced by 1-mM samples giving a signal-to-background of 10/1 (38).

Data Analysis

Edge spectra were analyzed by the methods described by Powers et al. (22). Absolute error in energy calibration is ±0.5 eV, but the relative error is ±0.1 eV. Final EXAFS spectra consisted of the average of many single scans. Before averaging, each scan was examined for unusual features, satisfactory signal-to-noise, and edge position in energy. Monochromator settings were converted to energy values and a linear background, which set the absorption below the edge to zero, was subtracted. Examples of copper and iron spectra for the fully oxidized state are given in Fig. 4.

The EXAFS modulation of the absorption is given by the equation:

$$\chi(k) = \sum \frac{-N_i |fi\,(k, \pi)|}{kr_i^2} e^{-r_i/\lambda(k)}\, e^{-2\sigma_i(k)k^2} \sin\{2[kr_i + \alpha_i(k)]\} \qquad (1)$$

where the sum is over the distances r_i from the absorbing atom, N_i is the number of the same type of backscattering atoms at r_i, $\lambda(k)$ is the photoelectron mean free path, and $f_i(k, \pi)$ is the backscattering amplitude of the ith atom which is $\sim Z/k^2$, for $k > \sim 4$ Å^{-1}. $\sigma^2(k)$ is the Debye-Waller factor describing the mean square displacement in r_i (from the thermal and lattice disorder), $\alpha_i(k)$ is the energy-

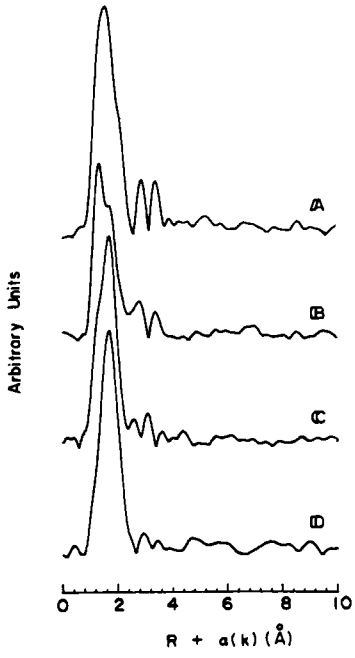

FIGURE 7

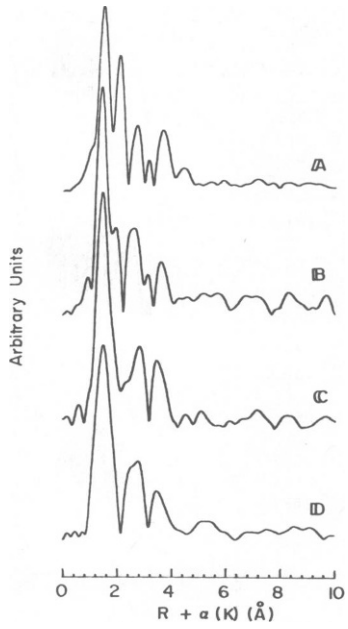

FIGURE 8

FIGURE 7 Fourier-transformed copper EXAFS data of the *A*, fully oxidized; *B*, mixed valence formate; *C*, mixed valence CO; and *D*, reduced CO states.

FIGURE 8 Fourier-transformed iron EXAFS data of the *A*, fully oxidized; *B*, mixed valence formate; *C*, mixed valence CO; and *D*, reduced CO states.

dependent phase shift of the photoelectron caused by the potentials of both the absorbing and the backscattering atom. k is the magnitude of the photoelectron wave vector given by

$$k = [2m_e (E - E_0)]^{1/2}/\hbar$$

where m_e is the electron mass, E is the x-ray energy and E_0 is the edge energy or threshold.

$\chi(k)$ was isolated from the data (Fig. 4) by a cubic B-spline fit to remove the "isolated atom" contribution. The results were then multiplied by k^3 to compensate for the $1/k^3$ dependence of $\chi(k)$ for $k > \sim 4$ Å^{-1}. This somewhat equalizes the oscillations in the observed range of k. This function was then normalized to one absorbing atom by the magnitude of the edge. These data for both copper and iron EXAFS are shown in Figs. 5 and 6. The $k^3\chi(k)$ data was Fourier transformed without smoothing or the use of a filter function, since the data clearly have sufficient signal-to-noise ratio to use directly (three times that of the hemoglobin data [27, 39]) and it was unnecessary to sacrifice resolution to obtain it artificially. Fourier transforms of the data of Figs. 5 and 6 are shown in Figs. 7 and 8. [Note that the abscissa contains contributions from the absorber-scatterer phase shifts, $\alpha(k)$]. Contributions of the individual resolved shells to the $k^3\chi(k)$ data of Figs. 5 and 6 are obtained by Fourier filter and are referred to throughout this paper as filtered data of a particular shell (Fig. 9). These data for each shell were then decomposed into a unique solution of an amplitude and phase.

The phase is unique to the absorber-scatterer pair. This has been experimentally as well as theoretically proven to be "chemically transferable" from the chemical environment of one compound to another (40). The amplitude, which contains N_i, $\sigma(k)$, and $\lambda(k)$, on the other hand, has proved to vary as much as 50% due to the chemical environment and inelastic scattering effects (41). For this reason, only the phase was used to identify the chemical type of a scattering atom (one type per shell) and the amplitude then tested (41–42) to be the same as that of the model within small variation of N_i and/or $\Delta\sigma^2$. All shells containing multiple types of atoms and distances were identified by direct comparison of filtered data with that of model compounds with no fitting procedures or variables. In this manner, the serious pitfalls yielding erroneous results of curve fitting to either the total $k^3\chi(k)$ data (44) of Figs. 5 and 6 or the filtered data of a single shell (Fig. 9) were completely avoided.

A comprehensive review on data analysis procedures is given by Lee et al. (42) and Powers (43).

RESULTS AND DISCUSSION

Cytochrome Oxidase Samples

Four sets of data are discussed here. The first two sets verify that cytochrome oxidase and its derivatives are authentic and the third set verifies that they are maintained so throughout the

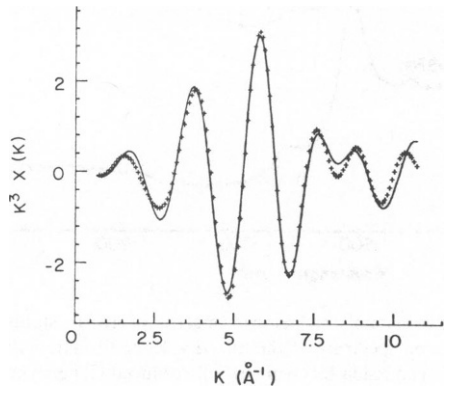

FIGURE 9 Copper first-shell filtered data of the mixed valence formate state (—) and the sum of oxidized stellacyanin (Cu_{a_3}) and reduced Cu_a contributions (+).

interval of x-ray observation. These data are followed by the results on edge and EXAFS studies.

Verification of Derivatives

Fig. 1 gives the absorption spectra of oxidized and reduced cytochrome oxidase under the usual conditions of assay: that of transmission in a liquid sample. Fig. 10 *C* illustrates a typical transmission spectrum through the sample at a concentration employed in the edge and EXAFS studies. In this case, for the most concentrated samples, attenuation of the light in the near-ultraviolet region is so high that only wavelengths >500 nm are shown. Thus, the spectrum in the oxidized state gives only the α-band corresponding to a and a_3 hemes, plus the

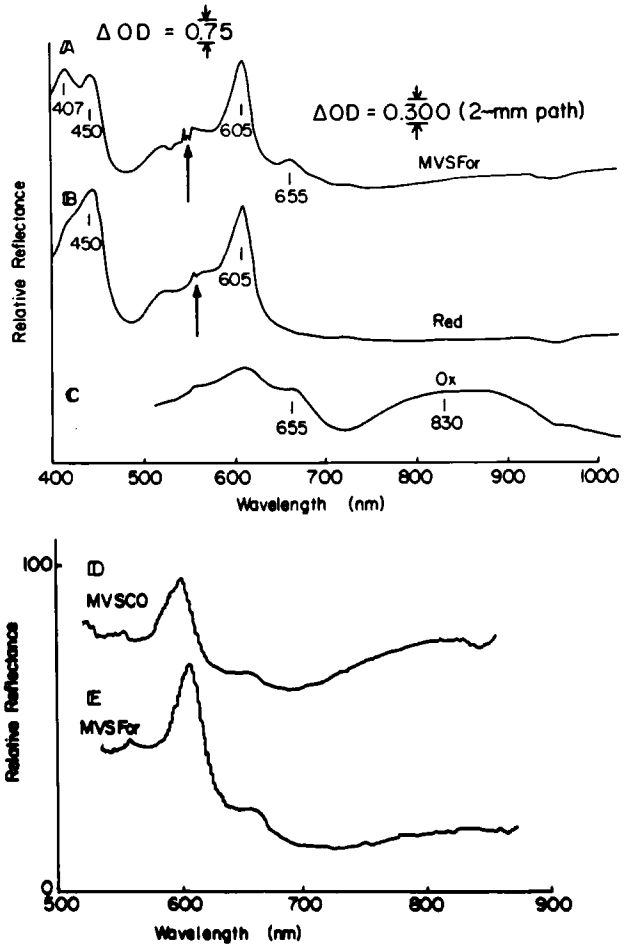

FIGURE 10 Optical transmission and reflectance spectra of redox states of cytochrome *c* oxidase (~1.0–1.5 mM); *A*, transmission spectrum of the mixed valence formate hybrid (MVS For) (zero point o.d. is 0.365 at 980 nm); *B*, transmission spectrum of fully reduced CO enzyme (zero point o.d. is 0.365 at 980 nm); *C*, transmission spectrum of the oxidized enzyme (zero point o.d. is 0.697 at 980-nm); *D*, and *E*, reflectance spectra of mixed valence CO (MVS CO) and mixed valence formate samples of cytochrome oxidase as prepared from the procedure described in the text.

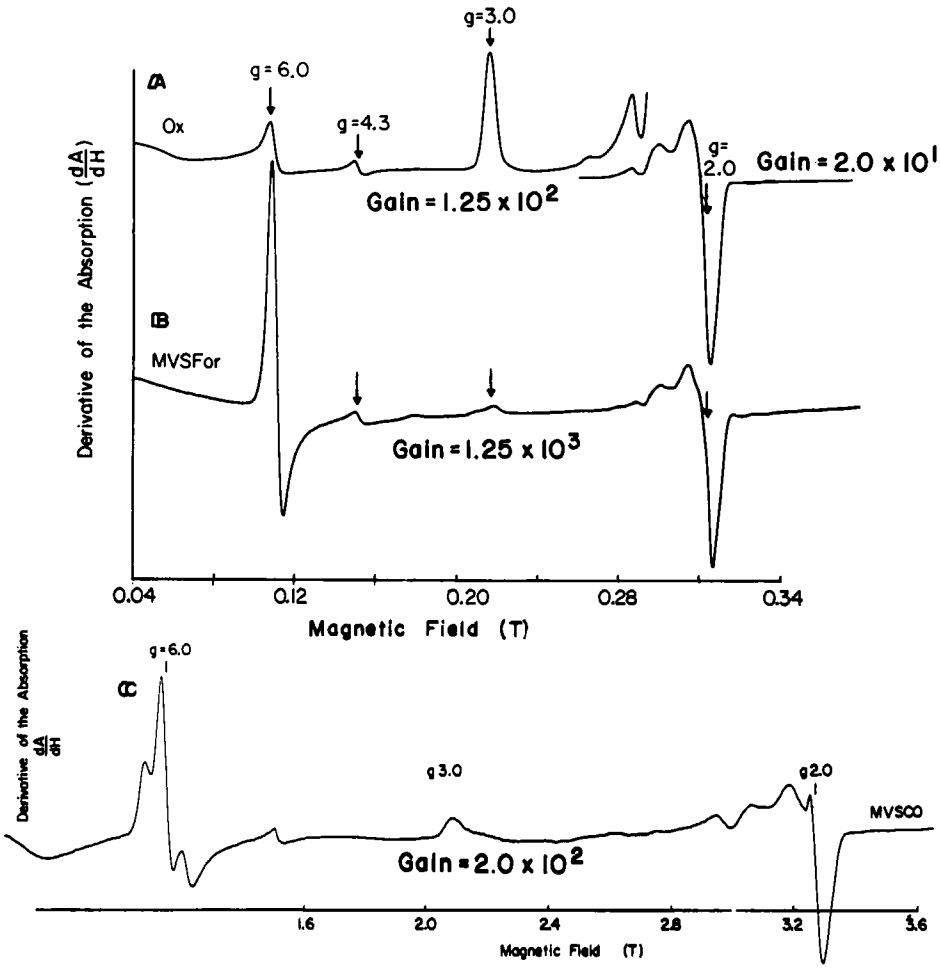

FIGURE 11 EPR derivative spectra of the redox states of cytochrome *c* oxidase (1.0–1.5 mM) *A*, fully oxidized enzyme (Cu region: gain = 2×10^1); Fe region: gain = 1.25×10^2); *B*, mixed valence formate hybrid (gain = 1.25×10^3); *C*, mixed valence CO hybrid (gain = 2.0×10^2). The following parameters were the same for all spectra: power 10 mW, modulation frequency 100 kHz, modulation amplitude 1 mT (T = 10K).

near-infrared band corresponding to the copper bands. Of particular interest is the 655-nm band that serves as a marker for $a_3{}^{+3}$ hemes (45).

Conversion to the mixed valence formate state, Fig. 10 *A* (45) causes a drop of the 830-nm band to about 15% of its initial value, leaves the 655-nm band unchanged, and causes an increase of the 605-nm band to approximately half its maximum intensity. The Soret band is split since it contains both oxidized a_3 heme at 418 nm and reduced *a* heme at 445 nm. While the residual absorption at 830 nm of the mixed-valence formate could be attributed to lack of complete reduction of the Cu_a component, Powers et al. (22) and Beinert et al. (46) suggest that ~15% of the total absorption at 830 nm could be attributed to Cu_{a_3}.

The CO-reduced samples (Figure 10 *B*) show no absorption bands at 830 and 655 nm, while the 605-nm band is largely due to the contribution of the *a* heme component with a

small contribution from the a_3 heme + CO component at 590 nm. The Soret band was split due to the separate positions of *a* heme and a_3 heme + CO at 445 and 430 nm, respectively.

The mixed valence CO compound shows an 830-nm band (Fig. 10 *D*) due to oxidized Cu_a. However, there is a distinctive shoulder a 655 nm which shows oxidized a_3 heme remaining. An evaluation of the amount of this residual oxidation is afforded by a comparison of this spectrum with that of the mixed valence formate Figure 10 *E* (recorded under identical conditions) which shows a strong 655-nm shoulder, with a small 830-nm band. The α-band of the mixed valence state CO shows a shift toward 590 nm with respect to mixed valence state formate. Assuming that the mixed valence formate corresponds to 100% oxidation of a_3 heme, we estimate that as much as 40% of a_3 heme remains oxidized in this particular mixed valence CO sample.

To verify the mixed valence state hybrids by other than optical means, EPR spectroscopy was used. Fig. 11 *A*, *B*, and *C* shows X-band (~9 GHz) absorption derivative spectra of the oxidized, mixed valence formate, and mixed valence CO hybrids, respectively. In Fig. 11 *A* and *B*, the EPR spectrum of the fully oxidized enzyme is compared to the mixed valence formate complex. The fully oxidized enzyme exhibits a low spin $g = 3.0$ signal and $g = 2.18$, and $g = 2.00$ signals, indicative of a^{3+} heme and Cu_a^{2+} respectively. The spectra also show a $g = 6.0$ signal attributable to a partially reduced high spin species. Quantitation (47) showed this species as $\leq 5\%$ of the *a* heme spin concentration. The mixed valence formate spectra reveal an axial $g = 6.0$ signal concomitant with the disappearance of the low spin $g = 3.0$ *a* heme signal. Quantitation shows that this $g = 3.0$ signal represents $<5\%$ of the high spin species. The resonance Raman studies (48) of Babcock suggest the nature of the high species to be due to a_3^{3+} heme $-$HCOOH.

Figure 11 *C* shows the EPR spectrum of the mixed valence CO complex. It exhibits an oxidized *a* heme signal at $g = 3.0$. It also shows two high spin species, one nearly axial, and the other rhombic (49). These species represent 15–20% of the total heme concentration. These high spin species represent incomplete conversion to the carbon-monoxy complex.

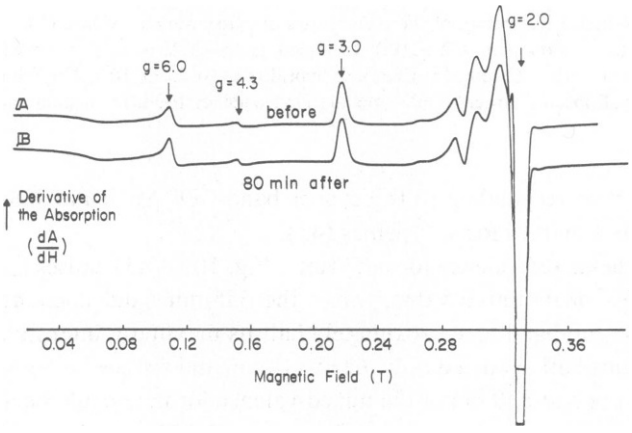

FIGURE 12 EPR derivative spectra of fully oxidized cytochrome *c* oxidase (1.0–1.5 mM), *A* before and *B*, after irradiation (~80 min irradiation time). Power 10 mW, T = 10K, gain = 1.25×10^1, modulation amplitude = 1 mT.

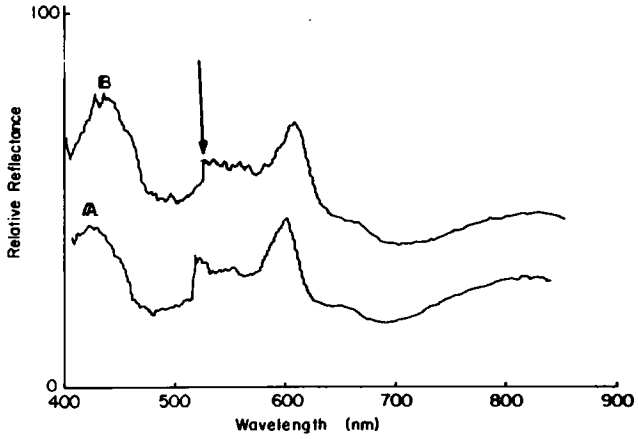

FIGURE 13 Reflectance optical spectra of the mixed valence formate state, *A*, before; and *B*, after 70 min irradiation (T = 120°C). Arrow indicates placement of second-order cut-off filter.

Effects of X-irradiation

Samples were monitored after every 30 min of beam exposure, and changed whenever a >10% alteration of the optical spectrum was detected. EPR spectra of the oxidized state before and after irradiation are shown in Fig. 12. The figure shows that 80 min of irradiation at −130°C causes a scarcely detectable change of EPR signals due to the trapping of hydrated electrons and free radical components at this low temperature (35). There is no change within experimental error of the $g = 3$ signal attributed to a heme or the $g = 6$ signal, representing

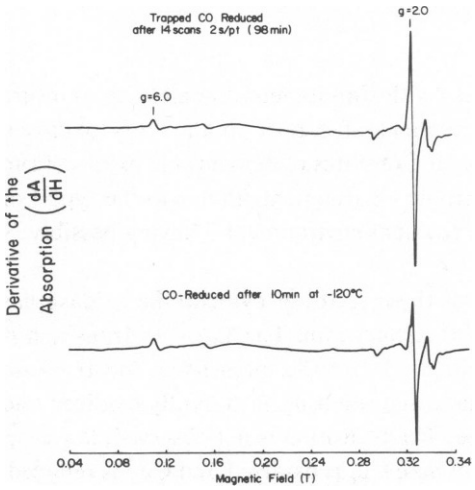

FIGURE 14

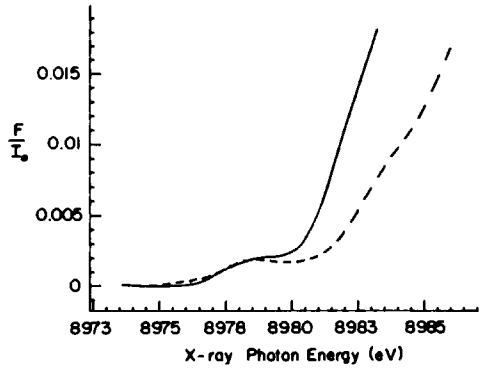

FIGURE 15

FIGURE 14 EPR derivative spectra of reduced cytochrome *c* oxidase (1.0–1.5 mM) rapidly quenched in liquid nitrogen after irradiation (top) and after a 10-min equilibration at −120°C (bottom).
FIGURE 15 1s → 3d transition region of the copper absorption edge of fully oxidized state normalized to one Cu atom and oxidized stellacyanin normalized to 0.5 Cu atom.

<5% of the *a* heme-spin concentration. The $g = 2$ signal shows an increase in the trapped radical concentration (as discussed below). Optical data under the same condition show a clear 830-nm infrared band and a 655-nm band, characteristic respectively of oxidized copper and a_3 heme. The effect of 70 min irradiation upon the mixed valence state formate (Fig. 13) causes a diminished 830-nm band of ~40%, and data obtained with such a sample were not used in the analysis.

Trapped Radical Generation

Reduced cytochrome oxidase used in Fig. 14 shows no $g = 3$ and scarcely detectable $g = 2$ and $g = 6$ signals. The sample was removed rapidly from the −130°C cryostat, plunged into liquid nitrogen, and examined by EPR spectroscopy immediately thereafter at 10 K (Fig. 14). The sample was found to show a large signal due to trapped radicals. The free radical was unsaturated at 10 K and at a microwave power of 10 mW, indicating that some of the species could be near (5–20 Å) a magnetic relaxation agent, possibly another free radical or paramagnetic center. Quantitation of the $g = 2.0$ free radical species was estimated from an all-*trans* polyacetylene sample[2] of known spin concentration at 10 K. At the time of trapping (after 10–15 scans), the irradiated cytochrome *c* oxidase preparation contained a spin concentration of ~500 μM, about half that of the oxidase itself. The sample was then monitored spectroscopically at −120°C for 10 min to confirm that the reduction state of the copper components had been unaltered by the radical formation. Then the sample was returned to the helium dewar and reexamined, and a diminution of radical intensity of ~40% was found. This demonstrates that the accumulation of trapped radicals in the frozen samples is significant, and that their assay requires continuous maintenance at very low temperatures to avoid radical reactions which would obscure their otherwise high concentration in the irradiated sample (50).

X-Ray Absorption Edges

Powers et al. (22) reported their use of edge studies (with simultaneous monitoring to insure proper redox state) to probe the electronic environment of copper in the fully oxidized, reduced CO, and mixed valence formate, cyanide, and CO states of cytochrome oxidase from beef heart. They concluded that "Cu_{a_3} has an electronic environment similar to the type I or 'blue' copper of stellacyanin" and "Cu_a has a more covalent environment," having possibly N (or O) and S^- as ligands.

In these studies, the 1s → 3d transition region of these states of cytochrome oxidase has been further investigated and compared with that of stellacyanin. The 1s → 3d transition is forbidden by the selection rules and when observed, is ~1% of the intensity of the 1s → 4p transition. This transition is identical in energy, shape and intensity in the fully oxidized and mixed valence formate states where Cu_{a_3} is oxidized. The transition is not observed, however, in the reduced CO state or mixed valence CO state where Cu_a is oxidized and Cu_{a_3} is reduced. Fig. 15 compares the 1s → 3d transition region of the fully oxidized state normalized to one Cu atom and oxidized stellacyanin normalized to 0.5 Cu atoms. The two are identical to

[2]Sample donated by A. G. MacDiarmid, Chemistry Department, University of Pennsylvania.

within our relative error of ±0.10 eV. Failure to observe this transition in the mixed valence CO state indicates the "covalent" nature of the Cu_a by comparison with the model compounds (22) and rules out the possibility that Cu_a is also a blue type I or a "super blue" copper (51) since all the investigated blue copper proteins, e.g., azurin, plastocyanin and stellacyanin, exhibit a 1s → 3d transition in the oxidized form. Further, azurin and plastocyanin have nearly identical edge features whereas stellacyanin is similar but not identical, indicating slight structural differences (52).

Cytochrome oxidase prepared from other sources is also investigated in the fully oxidized state. These sources include *Paracoccus denitrificans* (31) and thermophilic bacteria (HB-8) (32). These edge spectra are identical in every respect to that obtained for the fully oxidized state from beef heart, suggesting that the charge density of both copper atoms from each of these three sources is identical. Since the charge density is sensitive to the number and chemical type of ligands, as well as to the geometry of the ligands, this result suggests that all the copper sites are structurally identical. This similarity will be further addressed in the EXAFS section.

EXAFS

The EXAFS data, like that of the edge, are complicated by the fact that they are the sum of contributions from both copper sites in copper absorption data and both iron sites in the iron data. The approach of fitting just the phase with single atom pair contributions is futile because, for example, the first shells of the two Cu sites may contain eight or so neighbors with different distances and/or different chemical types. The only alternative is to model each site with a single compound. With this approach the mixed valence states (formate and CO) offer a unique method of changing one site while the other remains unchanged and, together with the fully oxidized and reduced CO states, offer a unique solution within experimental error to the contribution and identity of each site.

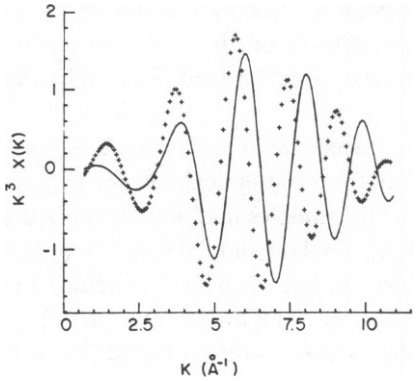

FIGURE 16

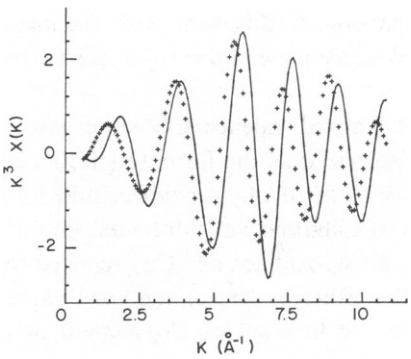

FIGURE 17

FIGURE 16 First shell filtered data of stellacyanin (Cu_{a_3}) normalized to 0.5 Cu atoms in the oxidized (—) and reduced (+) states.

FIGURE 17 First shell filtered data of the oxidized (—) and reduced (+) Cu_a contribution normalized to 0.5 Cu atoms.

Copper First Shell Contributions

Our copper edge studies (22) have provided unique insight into the identity of the copper sites: "Cu_{a_3} has a charge density similar to the type I or blue copper protein stellacyanin," and "Cu_a has a more covalent environment" having possibly N(O) and S^- as ligands. Using stellacyanin as a model for Cu_{a_3} in both the oxidized and reduced states (Fig. 16), we proceed in a manner analogous to that used for the edge data (22) to examine the first copper shells. The contribution of Cu_a to the fully oxidized state and reduced CO state can be determined by subtraction of the Cu_{a_3} model stellacyanin in the oxidized and reduced states, respectively. To do this, stellacyanin must first be multiplied by one-half. This is because all the data are normalized to one absorbing atom but cytochrome oxidase contains two coppers while stellacyanin contains only one. So, Cu_a(ox/red) = cytochrome oxidase (ox/red) − ½ stellacyanin (ox/red); where Cu_{a_3}(ox/red) = ½ stellacyanin (ox/red) and the redox state is given in parenthesis. The results are shown in Figs. 16 and 17.

Before we compare these results for Cu_a to model compounds, they must be tested for credibility with the data for the mixed valence states. In the case of the mixed valence formate state, an interference node is evident in the first shell of the Fourier transformed data (Fig. 7 *B*) and the filtered data (Fig. 9, $k \sim 8.5$ Å^{-1}). This pins the amplitudes and phases that contribute to this shell and provides a stringent critical test for whatever method is used to determine those contributions. Simply adding filtered data for Cu_{a_3} oxidized and Cu_a reduced (Figs. 16 and 17) produces a curve that is identical to the filtered protein data, particularly the interference node (Fig. 9). The deviation at large k is within the noise and truncation error that are largest in this region (Fig. 5). If the amplitudes and Debye-Waller factors for Cu_{a_3} and Cu_a are allowed to change, the comparison does not improve appreciably. Fitting the filtered protein data with a combination of two different types of atoms with average distances that are chemically reasonable and varying the number and Debye-Waller contributions does not produce nearly as good a fit (particularly to the interference node) as the sum in Fig. 9. If azurin (another blue copper protein with similar edge, EXAFS, and amino acid sequence at the copper site but not identical to those of stellacyanin) is used as a model for the Cu_{a_3} site, comparison of this sum with the protein filtered data is much worse, especially in the interference node region. The reasons for this difference are discussed in detail by Peisach et al.[3]

The mixed valence CO state where Cu_{a_3} is reduced and Cu_a oxidized is not as well characterized as the formate (Methods). It is clear from the optical spectra (Figure 10 *D*) that 35–40% of Cu_{a_3} is oxidized and not reduced for the samples used in these measurements. This contribution was subtracted from the filtered protein data and the result compared to the sum of Cu_a oxidized and Cu_{a_3} reduced (60%) as shown in Fig. 18. The comparison is identical for the distance (phase) and good but not identical for the amplitude. The difference can be eliminated by allowing Cu_a a small change in Debye-Waller contribution ($\Delta\sigma^2 < -3 \times 10^{-3}$ Å^2) indicating that at this site, the ligands are not bound as tightly as in the fully oxidized state. Other forms that are structurally different from the mixed valence CO state may be present in small amounts, and the small variation in Debye-Waller contribution may reflect

[3]Peisach, J., L. Powers, W. E. Blumberg, and B. Chance. 1981. Stellacyanin: structure of the metal binding site as determined by x-ray absorption spectroscopy. Submitted for publication.

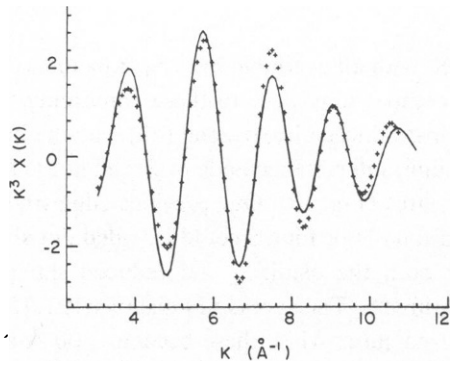

FIGURE 18

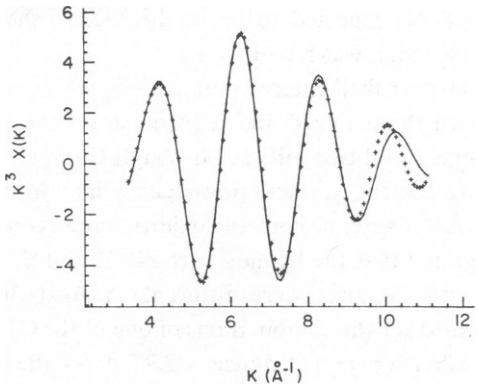

FIGURE 19

FIGURE 18 Cu first shell filtered data of the mixed valence CO state after subtraction of 40% oxidized stellacyanin (Cu_{a_3}, —) and the sum of 60% reduced stellacyanin (Cu_{a_3}) and oxidized Cu_a contribution (+).

FIGURE 19 First shell iron filtered data of the reduced CO (—) and mixed valence CO(+) states.

this. Studies are currently underway to determine which of these explanations is more accurate and to fully characterize this state at these high concentrations. Nevertheless, the comparison shown in Fig. 18 is good. The data can be fit nearly as well with a combination of nitrogen and sulfur ligands when the Debye-Waller contributions are not allowed to vary ($\Delta\sigma^2 = 0$). The reason for this agreement will be evident when the structure of the models is examined.

We conclude from these rigorous comparisons and requirements that allow only sums of model compound data that the nearest neighbors (first shell) of Cu_{a_3} have a structure identical to that of stellacyanin in both the oxidized and reduced states, i.e., the ligands and respective distances are the same. The filtered data obtained for Cu_a likewise represent the oxidized and reduced states.

In a recent study by Peisach et al.,[3] the EXAFS data of stellacyanin in both the oxidized and reduced states are compared to the crystallographic data of Coleman et al. (53) and Freeman et al. (54) for plastocyanin. The analysis of their data is identical to that employed here using the same model compound data for Cu-N and Cu-S contributions taken from copper (II) tetraphenylporphine (CuTPP) and copper (II) diethyldithiocarbamate (Cudtc) (55, 56), respectively. Although these results are presented elsewhere, their data for stellacyanin in the oxidized and reduced states are identical to that used for Cu_{a_3}; we will briefly summarize the results of their structure analysis. The first shell of stellacyanin was assumed to contain the same ligands as plastocyanin (54) and azurin (57) since the amino acid sequences are nearly identical (52). The oxidized form contains two N and one S, with an average of 1.97 Å[4] for N and 2.18 Å for S. A second shell contribution appeared to contain most likely S at 2.82 Å, but other likely candidates were N and C giving 2.95 Å. In the reduced state, 2.07 Å was found for one N and an average distance of 2.25 Å for two S. The

[4]All results presented here have ±0.03Å error unless otherwise stated.

second N, expected to be in the second shell from the comparison to reduced (low pH) plastocyanin, was not observed.

The first shell-filtered data for Cu_a was compared with all available model compounds, but in both the oxidized and reduced states the best comparisons were to those containing two nitrogens and two sulfurs. Although Cu butyraldehyde thiosemicarbazone (58) was the best, the agreement was not optimal, especially for the slight interference node observed in the k = 7–9 $Å^{-1}$ region of both the oxidized and reduced states (Fig. 17). Our previous edge studies suggested that the ligands were N(O) and S^-, and four N or four S could be ruled out since the edge features were different. A good fit for both the oxidized and reduced states is obtained for the combinations of one N (or O) and three S. The average N distance is 1.97 Å, and the average S distance is 2.27 Å for the oxidized state, while these become 2.00 Å and 2.35 Å, respectively, for the reduced state. A reasonable fit is also obtained for combinations of two N and two S but the average distances are the same within the error. The average distance is shorter for the oxidized and for the reduced states, when O is used instead of N, whereas the average sulfur distance is the same within experimental error. The large S content of this site is consistent with a more covalent environment than Cu_{a_3} (22) and with the EPR studies (59, 60).

The first shell contributions of copper can be summarized as follows: Cu_{a_3} is similar to stellacyanin in both the oxidized and reduced states. Cu_a is different from the blue copper proteins having more normal N or O and S bond lengths. Coordination numbers are one (or two) N or O with three (or two) S in both the oxidized and reduced states. The high sulfur content of this site is responsible for a more covalent environment than that of Cu_{a_3}.

Iron First Shell Contributions

Determination of the contributions of Fe_{a_3} and Fe_a are not quite as complicated as those for their functionally corresponding coppers since both cytochromes contain their irons in heme groups. Examination of the Fourier transformed data for the states shown in Fig. 8 reveals that the first shell of the fully oxidized and mixed valence formate states have very different contributions that those of the reduced CO and mixed valence CO states. The fully oxidized state has a split first shell that is almost completely resolved while that of the mixed valence formate state is similar but not as well resolved, since the signal-to-noise is not as good as that of the fully oxidized state.

Comparison of the first-shell filtered data of the reduced CO with mixed valence CO states indicates they are identical, as shown in Fig. 19. The optical spectra indicated <15% Fe_{a_3} was oxidized in the mixed valence CO state. The deviation at high k is within the errors and the experimental noise where these contributions are largest (Fig. 6). This result means that Fe_a changes very little structurally or not at all on a change in formal valence state (Fe_{a_3} is reduced for both states). It also means that the first shell of the fully oxidized state should be identical to that of the mixed valence formate state if the formate does not contribute to the Fe_{a_3} first shell or is not bound close enough to influence the structure. In catalase, the formate protons are known to reside ~9 Å from the iron (61), and only small contributions could be expected if this distance is as large in the mixed valence formate state. The split shells of the fully oxidized and the unresolved shells of the mixed valence formate states can be compared by several methods: comparison of the filtered data of both; treating the split shell as a single shell; comparing the filtered data of the partially resolved shells with a combination of the

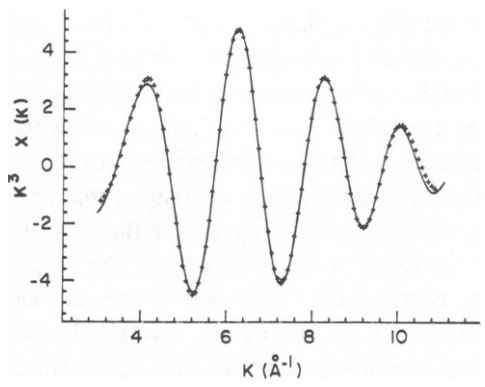

FIGURE 20

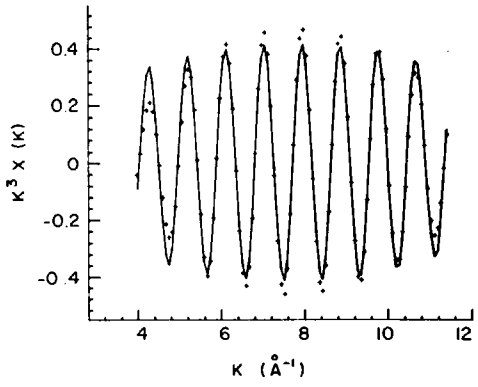

FIGURE 21

FIGURE 20 First shell iron filtered data of the reduced CO (—) state and the sum of oxyhemoglobin (Fe_{a_3}) and Im_2FeTPP (Fe_a) (+).

FIGURE 21 Third shell Cu filtered data of the fully oxidized state (mixed valence formate, —) and fit to one Fe atom ($\Delta\delta^2 \sim -3 \times 10^{-3}$ Å^2) (+).

filtered data of the two split shells of which each is treated as a single shell; or comparing the split shells and the partially resolved with a combination of models. All yield the same result. The mixed valence formate state contains a single contribution identical (±0.03Å) to the first of the split shells of the oxidized state and a contribution similar to that of the second of the split shells with a change of distance of −0.05 ± 0.05 Å. Within the error, the first shell of the mixed valence formate state is very similar if not identical to that of the combination of split first shells of the fully oxidized form.

Identification of contributions to first shells of the two Fe centers is now simplified since that of Fe_a does not change upon change in the formal valence, and both Fe reside in hemes. The problem is now to determine the axial ligands of the heme groups. There is considerable evidence (1, 10) that in the reduced CO state, CO (and also O_2) binds to Fe_{a_3}. In addition, histidine-type N are suggested as axial ligands for Fe_a from EPR (62), magnetic circular dichroism, and Raman studies (63, 23). The first-shell filtered data of several combinations of heme model compounds[5] and proteins (39) were compared with that of the reduced CO state (mixed valence CO). The sum of oxy-hemoglobin (HbO_2) and *bis* (imidizole)–α, β, δ, γ-tetraphenylporphinatoiron (III) Cl (Im_2FeTPP) (39)[5] reproduces the filtered data for the reduced CO state as shown in Fig. 20.

Oxy-hemoglobin has been shown to have an O at 1.75 Å, four heme N at an average distance of 1.99 ± 0.02 Å, and a proximal N at 2.07 Å (64, 39). This O distance is identical to those reported for heme iron carbonyls, and the EXAFS measurements cannot distinguish O from C. Im_2FeTPP has six N at an average distance of 1.986 Å. Thus, in the reduced CO state, Fe_{a_3} first shell is identical to oxyhemoglobin and Fe_a is identical to Im_2FeTPP in both the oxidized and reduced states. When the contribution of Fe_a is subtracted from the filtered data of the oxidized state (mixed valence formate), the remainder, which is the oxidized Fe_{a_3} contribution, contains a proximal N at 2.14 Å in addition to the four-heme N at 2.01 Å.

[5]Powers, L., J. C. Smith, J. S. Leigh, Jr., S. Srivastava, C. D'Ambrosio, and B. Chance. 1981. X-ray absorption edge studies of heme model compounds. Submitted for publication.

The second of the split peaks in the fully oxidized form is identified as S at 2.60 Å by the phase of the filtered data. Large changes in E_0(~12 eV) and poor fits are obtained when Fe-N, O, or C phases are used. When the filtered data are compared with that of Fe [CS_2: N − $(CH_2)_4$]$_3$ which contains six S at an average distance of 2.44 Å (65, 66); one S is found with only a small change in Debye-Waller contribution. As discussed earlier, this S is also present in the mixed valence formate state but is completely absent in the data of the reduced CO and mixed valence CO states. Although this distance is slightly longer than the usual octahedral S distance of ~2.45 Å, it is likely to be the sixth ligand of Fe_{a_3} for the following reasons: Addition of a sixth N(C, O) to the Fe_{a_3} contribution of the first of the split shells produces a significantly worse comparison. Model compounds (64) having a sixth N ligand do not produce as favorable a comparison. C and O are not likely to be the sixth ligand since, in axial heme ligands, the distance is usually significantly shorter (0.24 Å) than the average heme N distance and can be clearly recognized. At this distance, the S could not be a ligand of either the proximal N (or a second axial or sixth N, C, or O), since the shortest distance this Fe-N-S combination could be expected to give is >3 Å.

Results for iron first-shell contributions can be summarized as follows: Fe_{a_3} has an axial S ligand in the fully oxidized and mixed valence formate states which is replaced by CO in the reduced CO and mixed valence CO states, resulting in a structure similar to that observed in HbO_2 (and presumably HbCO). Fe_a changes very little, if any, on change in formal valence and is similar to Im_2FeTPP.

Higher Shell Contributions

As shown in Figs. 7 and 8 both the copper and iron data exhibit higher shells. Of particular interest is the distance between the Fe_{a_3} — Cu_{a_3} pair which are spin coupled in the fully oxidized and mixed valence formate states and may be present in the ≤~4 Å range observable by the EXAFS techniques. Several criteria are necessary for their identification in addition to favorable phase (and filtered data) comparisons. Each must be observed in the data of the other, i.e., Cu_{a_3} must be seen from Fe_{a_3} at the same distance Fe_{a_3} is seen from Cu_{a_3} in both the fully oxidized and mixed valence formate forms. The contribution must be able to be identified uniquely as Cu or Fe and not also as possibly N, C, O, or S or any of these in combination. Only when all these criteria are met by the same contribution can identification of these sites be reasonable.

Model compounds having a well-defined and characterized Cu-Fe distance in the observable range are not yet available. The phase and amplitude for such a pair was taken from models (19) having Cu-Cu distances such as Cu metal, [tmen-Cu(II)OH]$_2$ Br_2:tmen = *N, N, N, N*,-tetramethylethylenediamine, and Br_2[bpyCu(II)OH]$_2$ · SO_4 · $5H_2O$:bpy-bipyridyl. The phase of these models was then corrected for the absorbing or backscattering atom to be Fe instead of Cu by the difference of Fe and Cu contributions given by the theoretical phase calculations of Teo and Lee (67). Fe amplitudes were obtained by correcting the model amplitudes by the ratio of the Fe contribution to the Cu contribution obtained from the theoretical amplitude calculations of Teo and Lee (67). These Fe amplitudes were compared with those obtained from other Fe model compounds and found to be in excellent agreement. These corrections to the phase and amplitude of Cu-Cu phases and amplitudes were quite small, and Cu-Cu phase and amplitude could be used for those of Fe-Cu and Cu-Fe with little

difference or error. The phase and amplitude data of Cu metal that have been corrected for Fe as the absorbing or backscattering atom are referred to as corrected Cu metal data and were used to investigate the higher shells of both the iron and copper data of cytochrome oxidase.

From Fig. 7, it is clear that the higher Cu shells of the mixed valence formate state are similar to that of the fully oxidized while those of the reduced CO and mixed valence CO states are not. Comparison of the filtered data for these similar shells indicates that the third shells are identical but the second shells require a large change in E_0. Phase comparisons indicate that only the third shells contain Fe at 3.75 ± 0.05 Å (or Cu since the two cannot be distinguished), and comparison of the filtered data with that of corrected Cu metal data indicates one Fe ligand is present with very small change in Debye-Waller contribution ($\Delta\sigma^2 = \sim -3 \times 10^{-3}$Å^2). This comparison is shown in Fig. 21. In order to satisfy the remainder of our criteria, this contribution must also be present in the iron data.

The iron higher shells (Fig. 8) in all four states are similar to those observed in heme model compounds (68, 39), especially Im_2FeTPP and HbO_2. If this contribution at ~3.75 Å is present in the fully oxidized and mixed valence states, it is contained in the fourth (next to last) shells together with the N and C contribution of the heme groups at 4.12 ± 0.03 Å. Subtraction of this contribution for both hemes (Im_2FETPP model data Fig. 22 *A*) leaves the filtered data shown in Figure 22 *B*. Phase comparison shows this remainder contains only Cu (or Fe) at 3.75 ± 0.05 Å and comparison of the filtered data to that of the corrected Cu metal data shown in Fig. 22 *B* indicates one Cu is present with a small change in Debye-Waller contribution ($\Delta\sigma^2 = \sim -3 \times 10^{-3}$ Å^2). This contribution meets our criteria and can be

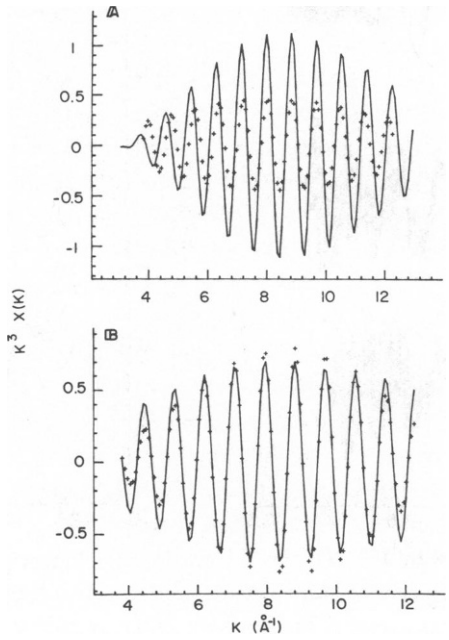

FIGURE 22 *A*, Fourth shell Fe filtered data of the fully oxidized state (—) and third shell Im_2FeTPP (+). *B*, Difference in (*A*) between oxidized state and Im_2FeTPP (—) and fit to one Cu atom ($\Delta\delta^2 \sim -3 \times 10^{-3}$ Å^2) (+).

identified as an Fe-Cu distance of 3.75 ± 0.05 Å. It is not possible that this could be the Fe_a-Cu_a distance since dipolar coupling at this distance would have dominated EPR properties (60). Fe_{a_3} and Cu_{a_3} are close enough to be spin coupled in their oxidized states while Fe_a and Cu_a are not. No other pair is discernable in the data.

Comparison of the iron fourth shells of the reduced CO and mixed valence CO states (Fig. 8) to Cu in the same manner did not produce results that could uniquely be identified as a single Cu. In fact, examination of all higher shells in all states for both the iron and copper data did not yield a unique identification of a metal atom. In addition, no higher shells are observed in the copper-reduced CO state (Fig. 7), and those of iron can be identified with known heme shells. The question then arises of what has happened to this metal atom pair in these states.

The fact that they are not observed can be due to any one or combination of the following reasons. The distance between them in the states where they are not spin coupled is larger than that observable (<~4 Å). The distance lies within the observable range but the loss of the bridging bond present in the oxidized states of this pair causes their mean-square displacement (Debye-Waller contribution) to be large and the resulting contribution unobservable. The signal-to-noise in the data is not sufficient, although it is somewhat comparable to that of the fully oxidized and mixed valence formate states where those contributions are observed.

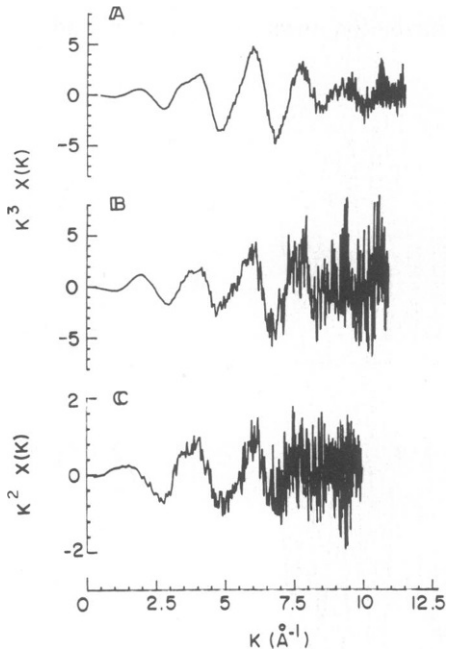

FIGURE 23

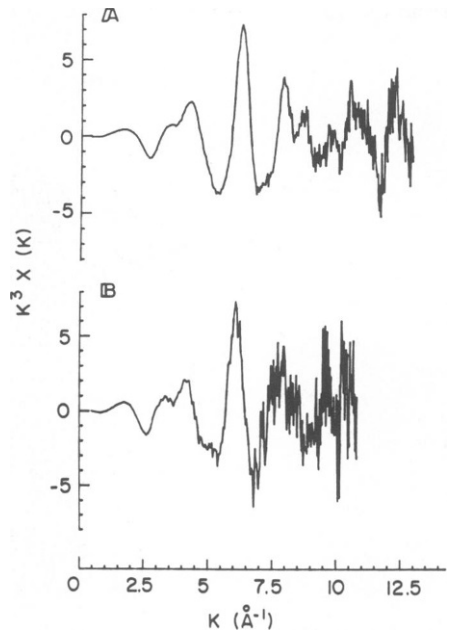

FIGURE 24

FIGURE 23 Background removed Cu EXAFS data multiplied by k^3 of the fully oxidized state of cytochrome oxidase from A, beef heart and *B, P.denitrificans* bacteria. *C*, HB-8 thermophilic bacteria background removed data multiplied by k^2.

FIGURE 24 Background removed Fe EXAFS data multiplied by k^3 of the fully oxidized state of cytochrome oxidase from *A*, beef heart and *B*, *P. denitrificans* bacteria.

Whatever the actual reason(s), the position of Fe_{a_3} relative to Cu_{a_3} is unknown when these centers are reduced and is currently under study.

Cytochrome Oxidase from Other Sources

In addition the the mammalian preparation from beef heart, those from *P. denitrificans* and HB-8 (thermophilic) bacteria were also studied in the fully oxidized form. Comparisons of these data with that of beef heart are shown in Fig. 23 for copper and Fig. 24 for iron. It is clear that these are similar. The copper data for HB-8 was multiplied by k^2 (giving the data a different appearance) instead of k^3 because this data did not have as good signal-to-noise. Comparison of the filtered data for the three shells of beef heart with *Paracoccus* gave identical contributions within experimental error. However, a small constant change in the Debye-Waller contribution ($\Delta\sigma^2 = \sim 3 \times 10^{-3}$ Å^2) was observed for each shell that indicated this structure was more rigid than that of beef heart. This result might be expected since this enzyme contains only two subunits instead of seven or so found for beef heart.

The data for beef heart were then analyzed with k^2 multiplication for comparison to that of HB-8. The first shells are identical within experimental error while the third shell distance was 0.05 ± 0.05 Å longer than that of beef heart, both having the same small change in Debye-Waller contribution as observed for *Paracoccus*. The Cu sites in cytochrome oxidase, whether from bacteria or mammals, are strikingly similar as suggested by the edge data given in the preceding section.

The iron contributions are also similar. Comparison of each shell with that of beef heart indicates they are identical within the experimental error and analysis of contributions using model compounds in the manner discussed for beef heart have identical results in all circumstances with small changes in Debye-Waller contributions.

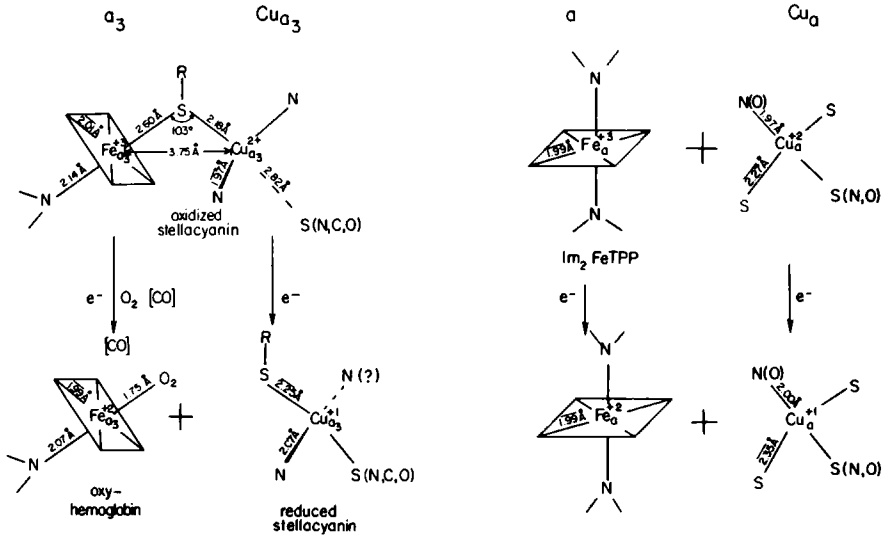

FIGURE 25 Pictorial representation of x-ray absorption results for the redox centers in the fully oxidized and reduced CO states. Other ligand possibilities are given in parentheses and (?) indicates ligands not observed but postulated from crystallographic data of similar models. Model compounds are identified where appropriate, error bars are omitted but given in text, and bars over distances indicate average distance for all the same type of ligands in that center.

We are left with the conclusion that the structure of these sites is so carefully engineered to their function, that of reducing molecular oxygen to water, that nature has conserved it! This surprising result may have far-reaching consequences when it is considered with respect to laccase and other oxidases, all of which have four redox centers but none of which contains both Fe and Cu (69). Let us now consider the overall structure of the sites and how they fit together.

SUMMARY

Redox Site Structure

A summary of the conclusions of this section is presented pictorially in Fig. 25. Model compounds are listed where applied. Dashed lines in the case of the Cu_{a_3} indicate ligands reported for plastocyanin (53, 54) and azurin (57) that are possibly too long to be real bonds. The N(?) in reduced stellacyanin indicates this ligand is not observed at all in our data. Other ligands contained in parentheses, e.g., (N, O), indicate other possibilities for the identity of this ligand. Error bars are not included for simplicity but are discussed in the preceeding text, and a line over the distance means the distance shown is an average of those for the same ligand in that metal center. The assignment of formal valence to a specific metal atom in the site is to indicate the oxidation state of the center, either oxidized or reduced, and does not mean that this total charge resides on the metal atom.

The active site Fe_{a_3}-Cu_{a_3} structure is unusual in that Cu_{a_3} closely resembles the blue copper protein stellacyanin of which the cysteine sulfur forms a bridging ligand to Fe_{a_3}. The sulfur is three liganded, having the same Cu—S cysteine bond length as stellacyanin, but an Fe—S distance longer than those usually observed for octahedral coordination. Cytochrome *c* (70), cytochrome *P*-450 (71), and similar models (66) lie in the range of 2.3–2.45 Å. The question then arises as to whether there exists a real bond from Fe to S. The average Fe—N (pyrrole) distance clearly resolves this question. High spin five coordinate hemes or models all contain $\geq$2.05 Å average distances, larger than our error of $\pm$0.03 Å. The only well-characterized high spin six coordinate model is metmyoglobin. The average Fe—N (pyrrole) distance is 2.04 Å when calculated for a flat heme (72, 64) but will be even shorter for a domed prophyrin (64). This is in good agreement with that observed for Fe_{a_3} oxidized as is the Fe—N (proximal) distance of 2.1 Å. However, intermediate spin states also have similar Fe—N (pyrrole) distances, but are characteristically 5-coordinate. We conclude that Fe_{a_3} oxidized is 6-coordinate and most likely high spin, similar to metmyoglobin.

Another striking feature is observed in this comparison. The axial O (H_2O) distance of metmyoglobin is 2.0 Å, ~0.25 Å longer than that of oxyhemoglobin or myoglobin (64, 39). The N (proximal) changes by ~0.05 Å. Similarly, the Fe_{a_3}—S distance is ~0.25 Å longer than that of cytochrome *c*, and the N (proximal) change is comparable. This lengthening of the axial ligands is caused partially by spin state change (73, 74) but further by the sixth coordination of the high spin iron (III). Model heme compounds (74) having various axial ligands, including sulfur, also display these characteristic changes. This long Fe_{a_3}—S bond certainly could be expected for six coordinate high spin Fe_{a_3}.

From the Fe_{a_3}—Cu_{a_3} distance in their oxidized states together with the Fe_{a_3}—S and Cu_{a_3}—S distances, the bridging sulfur bond angle is calculated to be ~103°. This is a

reasonable angle for the sp^3 bonding required for a sulfur having three ligands. This three-ligand geometry of sulfur might also be expected to cause a shift to higher energy and intensity reduction of the characteristic blue copper, S to Cu, change transfer absorption at 600 nm (75) from the Coulombic interaction with Fe_{a_3}.

The question of whether spin coupling can occur through the sulfur bridge is a difficult one. An early experiment is relevant; mercuration (and denaturation in urea) destroys the spin-coupling and brings the analytical and ERS determinations of copper into agreement (76). These results suggest a role of sulfur in spin-coupling. Even though the Fe—S bond is long, d orbitals can become extended, possibly allowing sufficient overlap. The overlap which would be most effective at long distances is the σ antibonding interaction of $Fe(d_{z^2})$ and one lobe of the $S(sp^3)$ configuration. The physical mechanism of this spin coupling requires further investigation, and can probably best be approached by models of this site.

Upon reduction of Cu_{a_3}, this center closely resembles reduced stellacyanin, and the bridging sulfur becomes a normal cysteine sulfur. The Fe_{a_3} center looses the bridging sulfur bond and binds CO or O_2 in a structure like oxy hemoglobin (77) and myoglobin. Although the remaining site of Fe_a and Cu_a is not as well determined with only average distances and uncertainty in the number and type of Cu_a ligands, only small changes with redox state are observed. The structure and changes of Cu_a are consistent with the edge and average distances observed for model compounds of similar structure. In addition, the high sulfur content of this site gives a "more covalent" environment than that of Cu_{a_3} and is consistent with the results of EPR techniques (59, 60). These facts, taken together, may be a consequence of their function as an electron donor or a reservoir site in the electron transfer mechanism. Fe_a remains low spin, and small changes (which are within our error ± 0.03 Å) should be associated with change in redox state as shown by Hoard (74, 75). The excellent agreement of Fe_a with Im_2FeTPP is not surprising, as it was suggested from EPR measurements by Blumberg and Peisach (62) and has been recently reported as a good model for the optical and Raman data as well (23, 63). The individual bond distances of Cu_a can only be approached by model compounds which satisfy the edge, EXAFS, optical, and magnetic resonance data for this site. With these structural features in mind, we will turn our attention to the impact of these structures upon the biochemistry and mechanism of cytochrome oxidase.

Biochemical Aspects

The existence of a six-coordinate high spin structure with an Fe_{a_3}—Cu_{a_3} S bridge affords an appropriate explanation for the lack of reactivity of the oxidized state to characteristic ligands (F^-, CN^-, N_3^-, SH^-, etc.) of peroxidase, metmyoglobin, and methemoglobin. The reactivity might be compared to that of cytochrome *c*, where methionine is the sixth coordination place of the Fe or to *P*–450, where Fe—S is involved. Certainly, the increased reactivity of the Fe^{+2} state as compared with the Fe^{+3} to ligands that usually react with the Fe^{+3} state, is consistent with one of the original observations: "The species of cytochrome oxidase inhibited by cyanide is present in large concentrations in the reduced systems, in low concentrations in the steady-state oxidized system, and in very low concentrations in the fully oxidized systems" (78, 79). The structure depicted in the Fig. 25 would be unreactive toward ligands until the Fe—S bond is broken. Then the reduced form avidly reacts with appropriate ligands,

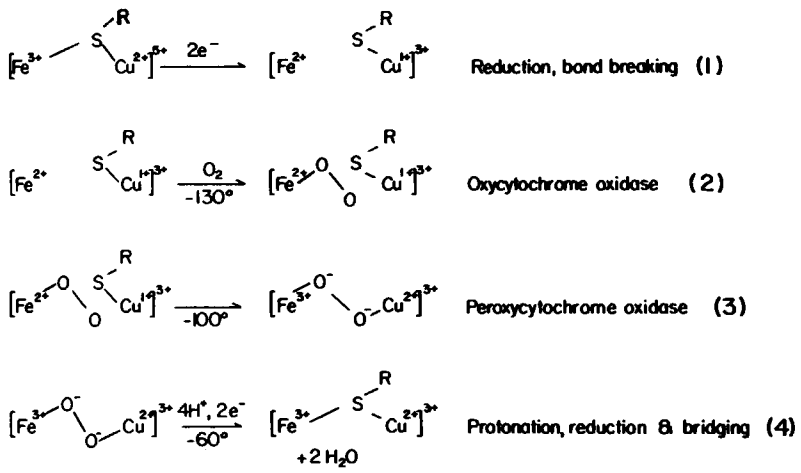

FIGURE 26 Model of proposed cyclic mechanism of oxygen reduction.

particularly oxygen and CO ($k_{O_2} \sim 10^8\ M^{-1}\ s^{-1}$) for which the enzyme has been specifically adapted.

The acceptance of a pair of electrons by the resting state from the electron transmitter portion, Cu_a and Fe_a, is an appropriate trigger for Fe—S bond rupture (Fig. 26, Eq. 1). The physiological electron donor is $Fe_a + Cu_a$, the structure of which seems ideal for electron transfer, presumably by a tunneling mechanism from $Fe_a + Cu_a$ to $Fe_{a_3} + Cu_{a_3}$.

The distance between cytochrome *c* and the $Fe_a + Cu_a$ site is indicated by resonance energy transfer to be ~25 Å (80). At ~ −60°C, cytochrome *c* is an effective electron donor directly to the active site, $Fe_{a_3} + Cu_{a_3}$. The distance between $Fe_a + Cu_a$ site and the active site must be considerable as well, although it has not been directly measured.

This process may take place in two one-electron–one-step reactions or in one two-electron step. For example one electron accepted by the Fe_{a_3} causes its reduction. Such an electron could be transmitted over the S-bridge to Cu_{a_3}, and a second electron from $Fe_a + Cu_a$ could then be accepted resulting in sequential reduction of both Fe_{a_3} and Cu_{a_3}. Since electron transfer into the redox center is probably rate-limiting, intermediate one-electron reduction steps have not been observed. However, the configuration of compound C described elsewhere[6], supports a $Fe_{a_3}^{+2} + Cu_{a_3}^{+2}$ configuration observed in the reoxidation reaction.

Once the S-bridge has been ruptured and a pair of electrons accepted, the active site reacts with oxygen with great avidity, the second-order constant approaching $10^8 M^{-1}s^{-1}$ at body temperatures and exhibiting, even at −130°C, a rate of 1 $M^{-1}s^{-1}$ (Fig. 26, step 2). The active site is not only appropriately structured to receive oxygen molecules rapidly, but the environment of this site is appropriate to occupancy with a significant number of oxygen molecules, even at low temperatures, as indicated by their competition with C_2H_2 and N_2O (81). Thus, Cu_{a_3} and its ligated S atom are not "in the way" of the oxygen reaction. Furthermore, as Alben et al. have suggested (82), the copper atom of the reduced state may accept CO as a ligand.

[6]K. DeFonseka and B. Chance. Manuscript in preparation.

a_3 heme under these conditions reacts similarly to hemoglobin and myoglobin with O_2. This is a remarkable conclusion, since it has been previously held that the unusual substituents on the green heme of cytochrome oxidase were particular to the oxygen reaction. However, this structural definition of the active site, plus observations that a protoporphyrin IX oxidase (cytochrome *o*) (83) exists as well, lend credence to the belief that the heme portion of cytochrome oxidase has no features that distinguish its initial reaction with oxygen from the well-known hemoglobins and myoglobins. This is further supported (13–15) by measurements of the dissociation constant for the O_2 reaction at low temperatures.

The apparent function of the binuclear complex is then, not to bind oxygen but to reduce it. The first step of oxygen reduction (Fig. 26, Step 3) is observed at ~ -100°C where electrons are transferred nearly simultaneously from $Cu_a + Fe_a$. No evidence of a one-electron intermediate has been observed when starting from the fully reduced oxidase, although this is not the case for the compound C as described below (84). The resulting intermediate, compound B $[Fe_{a_3}{}^{+3}—O^-—O^-—Cu_{a_3}{}^{+2}]^{+3}$, is strikingly similar to oxyhemocyanin $[Cu^{+2}—O^-—O^-—Cu^{+2}]^{+2}$, where the latter intermediate has a Cu—Cu distance of 3.68 ± 0.05 Å (19). The distance has not been determined for the carboxy ligated reduced cytochrome oxidase possibly because this structure is so flexible that the EXAFS signals are not observed. Nevertheless, the fact that the distance between Fe_{a_3} and Cu_{a_3} with the S-bridge is 3.75 ± 0.05 Å seems more than just coincidental, since both distances are exactly appropriate to the bridged peroxide structure. A number of resonance structures are possible, but compound B has characteristic absorption bands at 780 nm due to oxidized blue copper, together with absorbance decreases in the α and γ bands due to heme oxidation.

Compound C forms if the electron donation moiety $Fe_a + Cu_a$ is oxidized. Then, the copper absorption band is at 750 nm and a distinctive band due to sulfur to copper charge transfer is observed at 609 nm (84). The region of the Soret band shows no distinctive feature, and a liganding of the iron seems appropriate. Thus a possible structure is $[Fe_{a_3}{}^{+2}—0—0^-—Cu_{a_3}{}^{+2}]^{+3}$. Further studies of the interatomic distances in these two compounds will clarify the mechanism and the bridged peroxide structure now based in part on analogy and part on the interatomic distance of the resting state.

At -60°C, two more electrons are transferred from $[Fe_a{}^{+2} + Cu_a{}^{+1}]^{+3}$. A variety of intermediates can be involved at this stage, previously identified as higher valence states of cytochrome oxidase, particularly the ferryl ion, and indeed, cation radical species, etc. are possible (Fig. 26, Step 4). Protonation of the peroxide is an important part of these species, and is in accordance with measurements of protonation of compound B at temperatures about -40°C. Presumably these reactions could occur at lower temperatures, although the technique is not adequately developed for these studies.

The end product of the complete reduction of oxygen to water is not understood at the present time. One alternative is that the S-bridged $Fe_{a_3}{}^{+3} + Cu_{a_3}{}^{+2}$ complex characteristic of the resting state is reformed, and indeed this is the most probable structure. However, the structure of the reoxidized enzyme during catalytic activity has not yet been trapped.

Antonini et al. (85) find that the recycled oxidase is more active than the resting form. A structural explanation of this phenomenon rests in the possibility that the S-bridge may not have time to be reestablished during active electron transfer, and electrons may be accepted directly by the $Fe_{a_3}{}^{+3}$ and $Cu_{a_3}{}^{+2}$ by electron tunneling rather than by S-bridged electron transfer as proposed as the initial step of the reaction.

Relation to Other Oxidases and Transport Pigments

One of the remarkable conclusions of the correlation of structure and functional aspects of oxygen reduction by cytochrome oxidase is the superposition of the reduced O_2 (C) structure of the oxidase with that of oxy hemoglobin. The characteristic oxygen bond length is identical. This structural result agrees to a striking degree with the kinetic and thermodynamic properties of the oxygen compounds. Both are relatively highly dissociated, in fact, even more so in the case of cytochrome oxidase, where the dissociation velocity of oxygen extrapolated from the low temperatures studies to room temperature is very large. It appears, therefore, that there is nothing in either the structural or functional aspects of oxygen binding to cytochrome oxidase that explains its small oxygen requirement under physiological conditions. Thus, other factors are involved that distinguish cytochrome oxidase from oxygen transport pigments.

The proximal Cu_{a_3} affords a rapid electron donation to oxygen which, together with the a_3 heme, reduces oxygen to the peroxide state, overcoming in one two-electron step the energy barrier between the two states of oxygen reduction. At this point, however, cytochrome oxidase has accomplished nothing more than hemocyanin, which in its peroxy form closely resembles the postulated structure for compound B. The second difference is a physical one: neither hemoglobin nor hemocyanin contains the "electron reservoir" of cytochrome oxidase in the form of *a* heme and Cu_a that very rapidly donate a pair of electrons at room temperature and reduce both the oxy- and peroxy forms of cytochrome oxidase. Even with the most penetrating kinetic methods, (4, 5) no detectable concentration of these intermediates can be found.

The possibility of protoporphyrin IX serving as an effective oxidase component is suggested by the existence of cytochrome *o*, a protoporphyrin IX oxidase prevalent in many types of bacteria (83). In this case, however, the function of the enzyme involves relatively stable peroxide intermediates that no doubt interfere with its efficiency. In one special form, however,[7] cytochrome *o* replaces Fe_{a_3} + Cu_{a_3} and has associated itself with the electron reservoir system of cytochrome oxidase (*a* heme and Cu_a), which serves to reduce the iron peroxide compound in physiological function. Thus, manifold variations of the nature and function of oxygen reduction may occur, but the principles of operation are essentially those embodied in the paragraph above.

First, the remarkable features of cytochrome oxidase are the close homology between the a_3 heme and that of oxyhemoglobin, both forming a loosely bound oxygen intermediate. Second, in common with hemocyanin, a binuclear metal atom complex, in this case, Fe_{a_3} + Cu_{a_3} as compared with Cu—Cu, can bind oxygen and rapidly reduce it to the peroxide state. Third, and most distinctive, is the presence of the second pair of metal atoms, serving as effective reductants of oxygen to water. A fourth and novel feature, we believe, is the possibility of reducing the Cu_{a_3} by a S-bridged electron transfer from Fe_{a_3}. These remarkable features comprise a new perspective on the nature and function of cytochrome oxidase.

The authors thank J. Peisach, W.E. Blumberg, T.G. Spiro, and P. Eisenberger for their continued interest and helpful discussions. Beef heart cytochrome oxidase was prepared by J. Moore and S. Beer. Bacterial preparations were

[7]B. Chance, E. Yang, and N. Sone. Unpublished observation.

donated by B. Ludwig and J. Fee. Data collection was enhanced by the help of C. D'Ambrosio, B. Muhoberac, E. Yang, J.C. Smith, C.H. Barlow, G. Woolery, V. Yachandra, J. Cerino, K. Cantwell, and the Stanford Synchrotron Radiation Laboratory staff.
Grants received were: National Institutes of Health HL-18708, Specialized Center of Organized Research (SCOR) HL-15061, National Institute of General Medical Services (NIGMS), GM-27308, GM-27476, Stanford Synchrotron Radiation Laboratory Projects 341/423.

Received for publication 23 December 1980 and in revised form 5 March 1981.

REFERENCES

1. Warburg, O. 1949. Heavy Metal Prosthetic Groups and Enzyme Action. (Translated by A. Lawson) Oxford University Press, Oxford.
2. Keilin, D. 1966. The History of Cell Respiration and Cytochromes, Cambridge University Press.
3. Wharton, D. C., and A. Tzagaloff. 1963. A correlation of the near infrared absorption band of cytochrome oxidase with enzymatic activity and copper content. *Biochem. Biophys. Res. Commun.* 13:121–125.
4. Chance, B. 1967. The reactivity of haemoproteins and cytochromes. Second Keilin Memorial Lecture. *Biochem. J.* 103:1–18.
5. Gibson, C. Greenwood, D. C. Wharton, and G. Palmer. 1965. The reaction of cytochrome oxidase with cytochrome *c*. *In* Oxidases and Related Redox Systems, T. E. King, H. S. Mason, and M. Morrison, editors. John Wiley & Sons, New York. 591–603.
6. Beinert, H., and R. Shaw. 1977. On the identity of the high spin heme components of cytochrome *c* oxidase. *Biochim Biophys. Acta.* 462:121–130.
7. Bray, R.C. 1964. Quenching by squirting into cold immiscible liquids. *In* Rapid Mixing and Sampling Techniques in Biochemistry B. Chance, et al., editors. Academic Press, Inc. New York. 195–203.
8. Chance, B., D. DeVault, V. Legallais, L. Mela, and T. Yonetani. 1967. Kinetics of electron transfer in biological systems. *Nobel Symp. 5.* S. Claesson, editor. Interscience Press, New York. 437–468.
9. Hartridge, H. and F. J.W. Roughton. 1923. A method for measuring the velocity of very rapid chemical reactions. *Proc. R. Soc. London A.* 104:375.
10. Chance, B. 1953. The carbon monoxide compounds of the cytochrome oxidases. II. Photodissociation spectra. *J. Biol. Chem.* 202:397–406.
11. Chance, B., B. Schoener, and T. Yonetani. 1965. The low temperature photodissociation of cytochrome a_3^{2+}. CO. *In* Oxidases and Related Redox Systems T. King, H. Mason, and M. Morrison, editors. John Wiley & Sons, New York. 609–621.
12. Chance, B., N. Graham, and V. Legallais. 1975. Low temperature trapping method for cytochrome oxidase oxygen intermediates. *Anal. Biochem.* 76:552–579.
13. Chance, B., C. Saronio, and J. S. Leigh, Jr. 1975. Functional intermediates of the reaction of cytochrome oxidase and oxygen. *Proc. Natl. Acad. Sci. U.S.A.* 72:1635–1640.
14. Chance, B., and J. S. Leigh, Jr. 1977. Oxygen intermediates and mixed valence states of cytochrome oxidase: infra-red absorption difference spectra of compounds *A,B,C,* of cytochrome oxidase and oxygen. *Proc. Natl. Acad. Sci. U.S.A.* 74:4777–4780.
15. Chance, B., C. Saronio, J. S. Leigh, Jr., W. J. Ingledew, and T. E. King. 1978. Low temperature kinetics of the reaction of oxygen and solubilized cytochrome oxidase. *Biochem. J.* 171:787–798.
16. Okunuki, K., B. Hagihara, I. Sekuzu, and T. Horio. 1958. Studies on cytochrome system. *In* Proc. Int. Symp. on Enzyme Chemistry. Maruzen, Tokyo. 264–272.
17. Antonini, E., M. Brunori, C. Greenwood, and B. G. Malmstrom. 1970. Catalytic mechanisms of cytochrome oxidase, *Nature (Lond.).* 228:936–937.
18. Perutz, M. F. 1972. Nature of haem-haem interaction. *Nature (Lond.).* 237:495–499.
19. Brown, J. M., L. Powers, B. Kincaid, J. A. Larrabee, and T. G. Spiro. 1980. Structural studies of the hemocyanin active site. I. Extended x-ray absorption fine structure (EXAFS) analysis. *J. Am. Chem. Soc.* 102:4210–4216.
20. Schonbaum, G. R. and B. Chance. 1976. Catalase. *In* The Enzymes. P. Boyer, editor. Academic Press, Inc., New York. 13:363–408.
21. Blumberg, W. E., and J. Peisach. 1979. Some possible chemical and electronic states of cytochrome *c* oxidase and its intermediate redox states. In Cytochrome Oxidase T. King, Y. Orii, B. Chance, and K. Okunuki, editors. Elsevier/North-Holland, Amsterdam. 153–160.
22. Powers, L., W. E. Blumberg, B. Chance, C. H. Barlow, J. S. Leigh, Jr., J. Smith, T. Yonetani, S. Vik, J. Peisach.

1979. The nature of the copper atoms of cytochrome *c* oxidase as studied by optical and x-ray absorption edge spectroscopy. *Biochim. Biophys. Acta.* 546:520–538.

23. Babcock, G. T., P. M. Callahan, J. McMahon, M. R. Ondrias, and I. Salmeen. 1980. Selective enhancement by resonance raman spectroscopy of the heme chromophores *a* and a_3 in cyt. oxidase. *In* Symposium on Interaction between Iron and Proteins in Oxygen and Electron Transport. Airlie Virginia. Abstract V-11.
24. Palmer, G., G. T. Babcock, L. E. Wickery. 1973. A model for cytochrome oxidase. *Proc. Natl. Acad. Sci. U. S. A.* 73:2006.
25. Synchrotron radiation instrumentation: Proceedings of the National Conference on Synchrotron Radiation Instrumentation. Gaithersburg, Md. Ederer, D. L., and J. B. West, editors. 4–6 June 1979. Elsevier/North-Holland.
26. Steffens, G. J., and G. Buse. 1979. Chemical constitution and subunit function of polypeptide II from cytochrome-*c*-oxidase. *In* Cytochrome Oxidase T. King, Y. Orii, B. Chance, and K. Okunuki, editors. Elsevier/North-Holland, Amsterdam. 79–90.
27. Eisenberger, P., R. G. Shulman, G. B. Brown, S. Ogawa. 1976. Structure-function Relations in hemoglobin as determined by x-ray absorption spectroscopy *Proc. Natl. Acad. Sci. U. S. A.* 73:491–495.
28. Chance, B., P. Angiolillo, E. K. Yang, and L. Powers. 1980. Identification and assay of synchrotron radiation induced alterations on metalloenzymes and proteins. *FEBS (Fed. Eur. Biochem. Soc.)* Lett. 112:178–182.
29. Powers, L., W. E. Blumberg, Y. Ching, P. Eisenberger, B. Chance, C. Barlow, J. S. Leigh, Jr., J. C. Smith, T. Yonetani, J. Brown, T. Spiro, J. Peisach, S. Vik, J. Hastings, and M. Perlman. 1979. X-ray absorption edge and extended fine structure (EXAFS) studies of cytochrome *c* oxidase. *Biophys. J.* 25:(2 pt. 2) 43*a*.
30. Yonetani, T. 1960. Studies on cytochrome oxidase. I. Absolute and difference absorption spectra. *J. Biol. Chem.* 235:845–852.
31. Ludwig, B., G. Schatz. 1980. A two-subunit cytochrome *c* oxidase (cytochrome aa_3) from *Paracoccus denitrificans. Proc. Natl. Acad. Sci. U. S. A.* 77:196–200.
32. Fee, J., M. G. Choe, K. L. Findling, R. Lorence, and T. Yoshida. 1980. A Cytochrome c_1aa_3 Complex from the Plasma Membrane of *Thermus Thermophilus HB8.* Symposium on interaction between iron and proteins in oxygen and electron transport. Abstract VI-12. Airlie, Virginia.
33. Chance, B. 1957. Techniques for the assay of respiratory enzymes. *In* Methods of Enzymology S. P. Colowick and N. Kaplan, editors. Academic Press, Inc., New York. 273–328.
34. Yonetani, T. 1967. Cytochrome oxidase: beef heart. *In* Oxidation and Phosphorylation. Methods of Enzymology. vol. 10 R. Estabrook, and M. Pullman, editors. Academic Press Inc., New York 332–339.
35. Jen, C. K. 1960. Electron Spin Resonance Studies of Trapped Radicals. *In* Formation and Trapping of Free radicals. A. Bass, and H. Broida, editors. Academic Press, Inc., New York. 213–256.
36. Bienenstock, A., and H. Winick. 1979. Stanford Synchrotron Radiation Laboratory activity report, 79/03: III-2.
37. Stern, E., and S. M. Heald. 1979. X-ray filter assembly for fluorescence measurements of x-ray absorption fine structure. *Rev. Sci. Instrum.* 50:1579–1582.
38. Marcus, M., L. S. Powers, A. R. Storm, B. M. Kincaid, and B. Chance. 1980. Curved-crystal (LiF) x-ray focussing array for fluorescence EXAFS in dilute samples. *Rev. Sci. Instrum.* 51:1023–1029.
39. Eisenberger, P., R. G. Shulman, B. M. Kincaid, G. S. Brown, and S. Ogawa. 1978. Extended x-ray absorption fine structure determination of iron nitrogen distances in haemoglobin. *Nature (Lond).* 274:30–34.
40. Citrin, P. H., P. Eisenberger, and B. M. Kincaid. 1976. Transferability of phase shifts in extended x-ray absorption fine structure. *Phys. Rev. Lett.* 36:1346–1349.
41. Eisenberger, P., and B. Lengler. 1980. Extended x-ray absorption fine structure determinations of coordination numbers: limitations. *Phys. Rev. B.* 22:3551–3562.
42. Lee, P. A., P. H. Citrin, P. Eisenberger, and B. M. Kincaid. Extended x-ray absorption fine structure: its strengths and limitations as a structural tool. *Rev. Mod. Phys.* In press.
43. Powers, L. 1981. X-ray absorption spectroscopy: application to biological molecules. *Biochim. Biophys. Acta: Rev. Bioenergetics.* In press.
44. Tullius, T. D., P. Frank, and K. O. Hodgson. 1978. Characterization of the blue copper site in oxidized azurin by extended x-ray absorption fine structure: determination of a short Cu—S distance. *Proc. Natl. Acad. Sci. U. S. A.* 75:4069–4073.
45. Denis, M. 1977. The involvement of the fully oxidized state in cytochrome oxidase reaction with oxygen studied with the 655 nm band as a probe. *FEBS (Fed. Eur. Biochem. Soc.) Lett.* 84:296–298.
46. Beinert, H., R. W. Shaw, R. E. Hansen, and C. R. Hartzell. 1980. Studies on the origin of the near infrared (800–900 nm) absorption of cytochrome *c* oxidase *Biochem. Biophys. Acta.* 591:458–470.
47. Aasa, R., S. P. Albrecht, J. Falk, K. Lanne, and B. Vänngard. 1976. Epr signals from cytochrome *c* oxidase. *Biochim. Biophys. Acta.* 422:260–272.

48. Babcock, G., P. M. Callahan, M. R. Onbrias, and I. Salmeen. Coordination geometries and titrational properties of cytochromes *a* and a_3 in cytochrome oxidase from soret excitation Raman spectroscopy. *Biochemistry.* In press.
49. Hartzell, C., and H. Beinert. 1974. Components of cytochrome *c* oxidase detectable by epr spectroscopy, *Biochim. Biophys. Acta.* 368:318–338.
50. Chance, B., P. Angiolillo, and L. Powers. 1980. Free radical generation at −140° under Synchrotron irradiation. Stanford Synchrotron Radiation Laboratory. User's Meeting: 80-05:77–78.
51. Chan, S. I., G. W. Brudvig, C. W. Martin, and T. H. Stevens. 1980. Symposium on Interaction between Iron and Proteins in Oxygen and Electron Transport. Airlie, Virginia. Abstract V-9.
52. Bergman, C., E. K. Gandvick, P. O. Nyman, and L. Strid. 1977. The amino acid sequence of stellacyanin from the lacquer tree. *Biochem. Biophys. Res. Commun.* 77:1052–1059.
53. Colman, P. M., H. C. Freeman, J. M. Guss, M. Murata, V. A. Norris, J. A. M. Ramshaw, and M. P. Venkatappa. 1978. X-ray crystal structure analysis of plastocyanin at 2.7 Å resolution. *Nature (Lond.).* 272:319–324.
54. Freeman, H. C. 1980. Electron transfer in "blue copper proteins". Proceedings of XXI International Conference on Coordination Chemistry, Pergamon Press, New York. In press.
55. Reddy, T. R., and R. Srinivasan. 1965. EPR and optical studies in copper diethyldithiocarbonate. *J. Chem. Phys.* 43:1404–1409.
56. O'Connor, B. H., and E. N. Maslen. 1966. A second analysis of the crystal structure of copper (II) diethyldithiocarbonate. *Acta Crystallogr.* 21:828–830.
57. Adman, E. T., and L. H. Jensen. 1980. Structural features of azurin at 2.7 Å resolution. Bioinorganic chemistry: metals in biology. *Isr. J. Chem.* In press.
58. Blumberg, W. E., and J. Peisach. 1968. *Bis* (thiosemicarbazone) and other nitrogen and sulfur ligated complexes of copper (II). *J. Chem. Phys.* 49:1793–1802.
59. Hoffman, B. M., J. E. Roberts, M. Swanson, S. Speck, and E. Margoliash, 1980, Copper ENDOR of cytochrome *c* oxidase (EPR). *Proc. Natl. Acad. Sci. U. S. A.* 77:1452–1456.
60. Mims, W. B., J. Peisach, R. W. Shaw, and H. Beinert. 1980. Electron spin echo studies of cytochrome oxidase. *J. Biol. Chem.* 255:6843–6846.
61. Herschberg, R. D., and B. Chance. 1975. Optical and magnetic resonance studies of formate binding to horse liver catalase and sperm whale myoglobin. *Biochemistry.* 14:3885–3891.
62. Blumberg, W. E. and J. Peisach. 1971. A unified theory for low spin forms of all ferric heme proteins as studied by epr. *In* Probes of Structure and Function of Macromolecules and Membranes. B. Chance, T. Yonetani, and A. S. Mildvan, editors. Academic Press, Inc. New York. 215–229.
63. Babcock, G. T., G. T. van Stellandt, G. Palmer, L. E. Vickery, and I. Salmeen. 1979. Heme *a* models for cytochromes *a* and a_3 in cytochrome oxidase. *In* Cytochrome Oxidase T. E. King, Y. Orii, B. Chance, and K. Okunuki, editors. Elsevier Scientific Publishing Co., Amsterdam, The Netherlands. 105–115.
64. Perutz, M.F. 1965. Structure and mechanism of haemoglobin. *Br. Med. Bull.* 32:195–208.
65. Healy, P. C., and A. H. White. 1972. Structural studies in the Tris (*NN*-dialkyldithiocarbamato) iron (III) "cross over" system. *J. Chem. Soc. (Lond.). Dalton Trans.* 1163–1171.
66. Teo, B. K., R. G. Shulman, G. S. Brown, and A. E. Meixner. 1979. EXAFS studies of proteins and model compounds containing diameric and tetrameric iron-sulfur clusters. *J. Am. Chem. Soc.* 101:5624–5631.
67. Teo, B. K., and P. A. Lee. 1979. *Ab initio* calculations of amplitude and phase functions for extended x-ray absorption fine structure spectroscopy. *J. Am. Chem. Soc.* 101:2815–2832.
68. Collins, D. M., R. Countryman, and J. L. Hoard. 1972. Stereochemistry of low-spin iron porphyrins. I. his (imidazole)—tetraphemylporphinatoiron (III) chloride. *J. Am. Chem. Soc.* 94:2066–2073.
69. Andreasson, L. E., R. Branden, and B. Reinhammar. 1976. Kinetic studies of *Rhus vernicifera laccase. Biochim Biophys. Acta.* 438:370–379.
70. Takano, T., O. Kallai, R. Swanson, and R. E. Dickerson. 1973. The structure of ferrocytochrome *c* at 2.5 Å resolution. *J. Biol. Chem.* 248:5234–5255.
71. Cramer, S. P., J. H. Dawson, K. O. Hodgson, and L. P. Hager. 1978. Studies of the ferric forms of cytochrome P_{450} and chloroperoxidase by extended x-ray absorption fine structure: characterization of the Fe—N and Fe—S distances. *J. Am. Chem. Soc.* 100:7282–7290.
72. Takano, T. 1977. Structure of myoglobin refined at 2.0 Å resolution. I. Crystallographic refinement of metmyoglobin from sperm whale. *J. Mol. Biol.* 110:537–568.
73. Hoard, J. L. 1971. Stereochemistry of hemes and other metalloporphyrins. *Science (Wash. D. C.).* 174:1295–1302.
74. Hoard, J. L. 1975. Stereochemistry of porphyrins and metalloporphyrins. *In* Porphyrins and Metalloporphyrins. K. M. Smith, editor. Elsevier Scientific Publishing Co., Amsterdam, The Netherlands. 317–380.

75. Gray, H. B., and E. I. Solomon. 1981. The electronic structures of blue copper centers in proteins. *In* Copper Proteins. T. G. Spiro, editor. John Wiley & Sons, New York. In press.
76. Beinert, H., and G. Palmer. 1965. Copper in cytochrome oxidase. *In* Oxidases and Related Redox Systems. T. King, H. Mason, and M. Morrison, editors. John Wiley & Sons, New York. vol. 2. 585–590.
77. Perutz, M. F. 1969. The croonian lecture: the hemoglobin molecule. *Proc. R. Soc. Lond. B.* 173:113–140.
78. Chance, B. 1953. The carbon monoxide compounds of the cytochrome oxidases. III. Photodissociation spectra. *J. Biol. Chem.* 202:397–406.
79. Nicholls, P., K. J. H. van Buren, and B. F. van Gelder. 1972. Biochemical and biophysical studies on cytochrome aa_3. VIII. Effect of cyanide on catalytic activity. *Biochim. Biophys. Acta.* 275:279–287.
80. Vanderkooi, J. M., R. Landesberg, G. W. Hayden, C. S. Owen. 1977. Metal-free and metal substituted cytochromes *c*. Use in characterization of the cytochrome *c* binding site. *Eur. J. Biochem.* 81:339–347.
81. de Fonseka, K., and B. Chance. 1980. Oxygen kinetics of frozen cytochrome oxidase: the capacity of the oxygen pocket. *Biochem. J.* 185:527–530.
82. Alben, J. O., R. A. Altschuld, F. Fiamingo, P. Moh. 1980. Structure of the cytochrome oxidase (a_3) heme pocket. Low temperature FTIR spectroscopy of the photolyzed CO complex. *In* Symposium on Interaction between Iron and Proteins in Oxygen and Electron Transport. Airlie, Virginia. Abstract V-15.
83. Castor, L. N., and B. Chance. 1955. Photochem action spectra of carbonmonoxide inhibited respiration. *J. Biol. Chem.* 217:453–465.
84. Chance, B., C. Saronio, J. S. Leigh, Jr. 1979. Compound C_2 a product of the reaction of oxygen and the mixed valence state of cytochrome oxidase. *Biochem. J.* 177:931–941.
85. Antonini, E., M. Brunori, A. Colosimo, C. Greenwood, and M. T. Wilson. 1977. Oxygen 'pulsed' cytochrome *c* oxidase: functional properties and catalytic relevance. *Proc. Natl. Acad. Sci. U. S. A.* 74:3128–3132.